

Marshall University

Marshall Digital Scholar

---

Theses, Dissertations and Capstones

---

2019

## Smart Roads: Investigating Roadways as Energy Sources for Potential Application of In-Lane Charging

Dhruvalkumar Hitendrakumar Patel  
patel281@marshall.edu

Follow this and additional works at: <https://mds.marshall.edu/etd>



Part of the [Engineering Mechanics Commons](#), and the [Transportation Engineering Commons](#)

---

### Recommended Citation

Patel, Dhruvalkumar Hitendrakumar, "Smart Roads: Investigating Roadways as Energy Sources for Potential Application of In-Lane Charging" (2019). *Theses, Dissertations and Capstones*. 1250.  
<https://mds.marshall.edu/etd/1250>

This Thesis is brought to you for free and open access by Marshall Digital Scholar. It has been accepted for inclusion in Theses, Dissertations and Capstones by an authorized administrator of Marshall Digital Scholar. For more information, please contact [zhangj@marshall.edu](mailto:zhangj@marshall.edu), [beachgr@marshall.edu](mailto:beachgr@marshall.edu).

**SMART ROADS: INVESTIGATING ROADWAYS AS ENERGY SOURCES FOR POTENTIAL  
APPLICATION OF IN-LANE CHARGING**

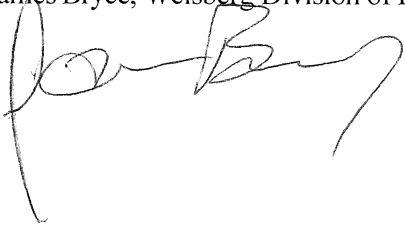
A thesis submitted to  
the Graduate College of  
Marshall University  
In partial fulfillment of  
the requirements for the degree of  
Master of Science  
In  
Transportation and Infrastructure  
Engineering  
by  
Dhruvalkumar Hitendrakumar Patel  
Approved by  
Dr. James Bryce  
Dr. Arka Chattopadhyay  
Dr. Gregory Michaelson

Marshall University  
December 2019

## APPROVAL OF THESIS

We, the faculty supervising the work of Dhruvalkumar Hitendrakumar Patel, affirm that the thesis, *Smart roads: Investigating Roadways as Energy Sources for Potential Application of In-lane Charging* meet the high academic standards for original scholarship and creative work established by the Master of Science Transportation and infrastructure engineering and the Marshall University. This work also conforms to the editorial standards of our discipline and the Graduate College of Marshall University. With our signatures, we approve the manuscript for publication.

Dr. James Bryce, Weisberg Division of Engineering



Committee Chairperson

Date

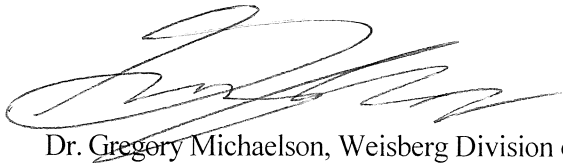
11/14/19

Dr. Arka Chattopadhyay, Weisberg Division of Engineering



Date

11/14/19



Dr. Gregory Michaelson, Weisberg Division of Engineering

14-Nov-2019

Date

© 2019  
Dhruvalkumar Hitendrakumar Patel  
ALL RIGHTS RESERVED

## **ACKNOWLEDGEMENT**

I want to acknowledge Dr. James Bryce. He helped with the MATLAB coding for the analysis which was very helpful to get an accurate result. Also, he helped me with the cost analysis of pavement. I would like to thank Sebastian Lopez for providing me the data about the energy consumption of the Marshall University Weisberg Applied Engineering Complex (WAEC). Moreover, I am thanking Federal Highway Administration (FHWA) because I have collected real wind speed, air density, and traffic data from FHWA's website.

## TABLE OF CONTENTS

<b>LIST OF TABLES</b> .....	vii
<b>LIST OF FIGURES</b> .....	viii
<b>ABSTRACT</b> .....	ix
<b>CHAPTER 1 INTRODUCTION</b> .....	1
<b>Road Pavements</b> .....	1
<b>Energy harvesting</b> .....	1
<b>Objectives</b> .....	1
<b>Source of energy</b> .....	2
<b>Charging of Electric Vehicles Technology</b> .....	3
<b>Outline of the thesis</b> .....	3
<b>CHAPTER 2 SUMMARY OF PREVIOUS STUDIES</b> .....	4
<b>Piezoelectric Material</b> .....	4
Carbon nanotube and nanofibers .....	5
Modeling .....	6
Conceptual Design of the Piezoelectric material in the pavement .....	8
Factors affecting the performance of energy harvester .....	10
Simplified Design for the piezoelectric transducer .....	10
<b>Wind turbine</b> .....	13
Darrieus turbine .....	14
Savonius wind turbine .....	15
H-rotor .....	16
<b>Solar Energy</b> .....	17
<b>Wireless Charging Technology</b> .....	17
Qualcomm HALO WEVC (Wireless Electric Vehicle Charging) .....	18
Level of charging .....	18
Level 1: 120 V AC .....	18
Level 2: 240 V AC .....	18
Level 3: DC Fast Charging .....	18
<b>CHAPTER 3 OVERVIEW ABOUT LOCATION</b> .....	19
<b>CHAPTER 4 NUMERICAL ANALYSIS</b> .....	20
<b>Piezoelectric material</b> .....	20
Formulas for the piezoelectric material .....	20
Capacitance .....	20
Static displacement .....	21
Static Voltage .....	21

Formulation .....	22
Results .....	24
Cost analysis.....	27
<b>Wind Turbine</b> .....	<b>30</b>
Conceptual Design of the wind turbine along the highway .....	30
Proposed Design.....	31
Analytical Analysis .....	31
Cost analysis.....	36
<b>Solar roadway</b> .....	<b>38</b>
Conceptual Design of the solar roadway.....	38
Road Surface layer .....	39
Electronic layer .....	39
Base Plate Layer.....	40
Analytical Analysis .....	40
Specification of Solar Panel .....	43
<b>CHAPTER 5 DISCUSSION AND CONCLUSION</b> .....	<b>44</b>
<b>Discussion</b> .....	<b>44</b>
Advantages of Piezoelectric materials .....	45
Disadvantage of Piezoelectric materials.....	45
Advantages of VAWT.....	46
Disadvantage of VAWT.....	46
<b>Conclusion</b> .....	<b>46</b>
REFERENCES.....	48
<b>APPENDIX A APPROVAL LETTER</b> .....	<b>51</b>
<b>APPENDIX B MATLAB CODING FOR PIEZOELECTRIC TRANSDUCERS</b> .....	<b>52</b>
<b>APPENDIX C MATLAB CODING FOR SENSITIVITY ANALYSIS</b> .....	<b>55</b>
<b>APPENDIX D MATLAB CODING FOR VAWT ANALYSIS</b> .....	<b>56</b>
<b>APPENDIX E PERMISSION CERTIFICATES</b> .....	<b>57</b>

## LIST OF TABLES

Table 1 Piezoelectric Constant (Jasim, Wang, Yesner, Safari, & Maher, 2017) .....	22
Table 2 Piezoelectric Transducer Specifications.....	25
Table 3 Piezoelectric Transducer Dimensions .....	26
Table 4 Strain Values for the Asphalt Pavement .....	26
Table 5 Power estimation from 20th Street to Hal Greer Blvd (0.5 miles).....	27
Table 6 Power estimation for Peak Hour .....	27
Table 7 Levelized cost for the piezoelectric material.....	29
Table 8 150W Poly Solar Panel Specification .....	43
Table 9 300W Poly Solar Panel Specification (CS6K-300MS) Recommended .....	43

## LIST OF FIGURES

Figure 1 Hierarchy of main energy harvesting technologies. (Caliò, et al., 2014).....	2
Figure 2 Cantilever arrangement with mass (Andriopoulou, 2012).....	8
Figure 3 Schematic of piezoelectric transducers embedded in a pavement (Jasim, et al., 2018).....	9
Figure 4 Schematic layout of the PZT transducer (Jasim, Wang, Yesner, Safari, & Maher, 2017) .....	10
Figure 5 Loading condition in Cymbal piezoelectric transducers (Zhao, Ling, & Yu, 2012).....	10
Figure 6 Loading condition in Bridge piezoelectric transducer (Zhao, Ling, & Yu, 2012).....	10
Figure 7 Structure of Piezoelectric Transducer (Zhao et al., 2014) .....	11
Figure 8 Location of a piezoelectric transducer (Najini & Muthukumaraswamy, 2016).....	12
Figure 9 Plate on elastic foundation subjected to moving distributed loads (Zhang, Xiang, & Shi, 2016) .....	12
Figure 10 Curved blade Darrieus VAWT (Tong, 2010) .....	15
Figure 11 Savonius type VAWT (Tong, 2010).....	16
Figure 12 H-rotor type VAWT.....	16
Figure 13 Intersection of 3rd avenue and Hal Greer Blvd .....	19
Figure 14 Cost as a function of the vehicle density (Guo & Lu, 2017) .....	28
Figure 15 Cross Section of Road with Wind Turbine (Malave & Bhosale, 2013).....	30
Figure 16 Helical Wind turbine (Kothe, Moller, & Petry, 2019).....	31
Figure 17 Distribution plot of wind velocity (V) .....	35
Figure 18 Distribution plot of air density rho.....	35
Figure 19 Distribution plot of power extracted from wind turbine .....	36
Figure 20 30-year Nominal Cash flow for wind turbine .....	37
Figure 21 Three layers of solar roadway (Northmore & Tighe, 2016) .....	38
Figure 22 Layers of Solar Roadways (Rahman et al., 2017).....	39
Figure 23 Model of solar panel (Rahman, Mahmud, Ahmed, Rahman, & Arif, 2017) .....	40

## **ABSTRACT**

The main aim of this thesis is to explore the potential for using pavements as part of energy harvesting infrastructure. Asphalt pavements can be used for multiple purposes such as for energy harvesting, eco-friendly use of the car, and the utilization of the natural renewable resources to produce electricity and that electricity use for in-lane charging technology which helps to charge a car when it is being driven on the road. The wireless charger is set-up under the asphalt pavement, and it will produce the magnetic field. The piezoelectric material and wind turbine are the electric source for applications such as the wireless charger. The solar roadways are included in the discussion but not considered as a source in this paper due to certain limitations. The analysis of power output from the piezoelectric transducers and helical wind turbine is calculated through MATLAB simulation. The results show significant promise for deriving energy from various sources along and in a roadway.

## CHAPTER 1 INTRODUCTION

### **Road Pavements**

Road pavements are structures comprised of layers of engineered materials on top of the natural soil subgrade, and their primary function is to distribute the applied vehicle loads to the subgrade. The pavement structure is designed to offer an acceptable surface in terms of adequate surface friction, favorable light-reflective characteristics, and low sound pollution. There are two types of pavements that are typically recognized: flexible and rigid pavements. This chapter provides information about road pavement, methods of energy harvesting, objectives, source of energy to convert into electrical energy, and charging technology.

### **Energy harvesting**

Energy harvesting from road infrastructure using a set of technologies that capture accumulated wasted energy that occurs in pavements and stores it for later use is the focus of study. Piezoelectric sensors, solar panels, solar thin film, and wind turbines are energy harvesting sources that have shown promise as detailed in chapter 2 of this thesis. Energy harvesting outputs are often listed as electrical energy production, heating, and cooling, deicing surfaces or powering wireless networks, or monitoring pavement conditions.

### **Objectives**

The objective of this thesis is to review the past research on pavements as energy harvesters and evaluate the feasibility of constructing a pavement with modern technologies for the purpose of forecasting energy and that energy going to be used for wireless charging of electric cars. For energy harvesting from piezoelectric material, Kirchhoff-Love's plate theory and sensitivity analysis were analyzed to check how much the strain affects energy production. For a wind turbine, the calculation is carried out based on idealized environmental conditions and actual wind data. In this thesis, multiple approaches to the results

have been included.

### Source of energy

There are several renewable energies available, such as solar panels, piezoelectric materials, wind turbines, and so on as shown in. We are not concerned about the solar technique that much in this paper, but the focus is the piezoelectric material and wind turbine.

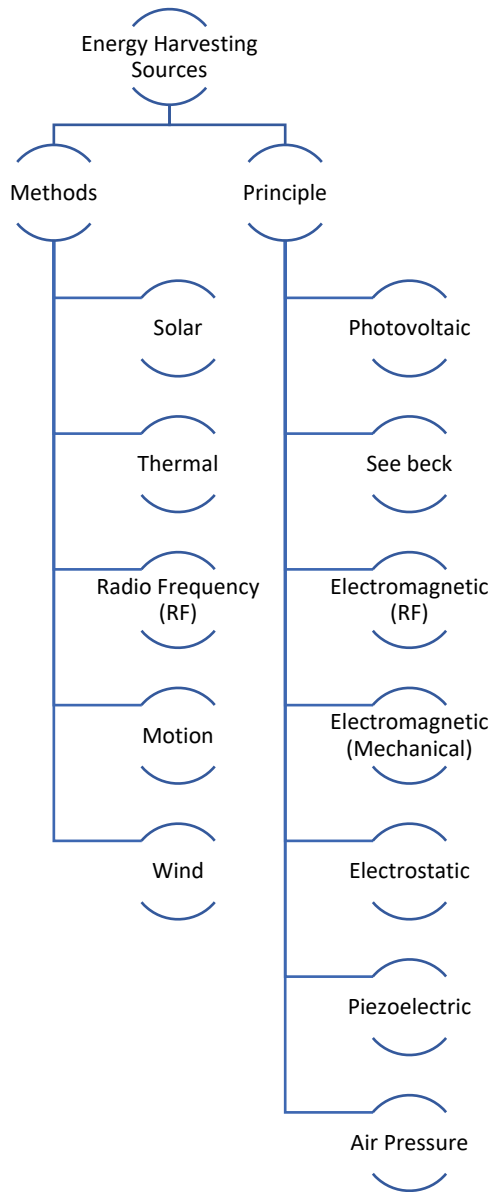


Figure 1 Hierarchy of main energy harvesting technologies. (Caliò, et al., 2014)

## **Charging of Electric Vehicles Technology**

The term Electric Vehicle Supply Equipment (EVSE) in a broader sense defines all the grounding and non-grounding equipment, electric vehicle connectors, attachment plugs, and all other kinds of accessories needed for charging of electric vehicles (Bansal, 2015). There are different types of charging ports and charging rates. Usually, the charging time range is less than thirty minutes to twenty hours or more, based on the type or level EVSE, the type of battery, and the capacity of the battery (Bansal, 2015).

## **Outline of the thesis**

Chapter 2 is about the summary of the previous researches related to this thesis paper. The overview and brief introduction of the location is covered in chapter 3. Chapter 4 is detail explanation of the numerical analysis and results of piezoelectric and wind turbines. Chapter 5 is discussion and it concludes the thesis based on the results. Also, codes for the MATLAB simulation and required permissions for the figures are attached in appendices respectively.

## CHAPTER 2 SUMMARY OF PREVIOUS STUDIES

This chapter presents the summary of past research on the energy harvesting methods from asphalt pavements. Chapter 2 includes the explanation of the method, formulas, and importance of previous papers in this thesis. Many of the papers have been written for small scale application such as pedestrian walkways. In this paper, the same applications have been used for a larger scale based on the dynamic force of the vehicle on asphalt pavement.

### **Piezoelectric Material**

Materials that produce energy through the vibrations are known as piezoelectric material (Caliò, et al., 2014). Duarte et al. (2003) explained the application to convert the kinetic energy to electric energy using the Waynergy system at small scale utilize under the pedestrian walkway. Waynergy system was developed by Waydip company in 2009 that converts the kinetic energy to the electric energy. Duarte et al. (2003) has done practical implementation of Waynergy system on the university access road pavement for the pedestrians. From this system, other few papers have been developed for larger scale application on the asphalt pavement such as energy harvesting from the highways. For example, Caliò et al. (2014) used finite element method to calculate the energy output from sources which does not explain work flow and how it works. The work flow and explanation of the formula are important and relevant to this thesis to compare the result with the MATLAB simulation.

Existing smart materials, such as piezoelectric ceramics, electroactive polymers, and shape memory alloys have various limitations holding them back from practical applications (Andriopoulou, 2012). The limitations center on the material's durability or size, and the material's range of strain force actuation. The carbon nanotube and nanofibers overcome the limitation of low electricity production because the carbon nanotubes help to boost the electricity output while the AC current is converting to the DC current. As shown in equation 1 and 2, the changes in the electric field, the electrical displacements, or mechanical

stresses and strains are linearly related.

$$T_{ij} = C_{ijkl}S_{kl} - e_{kij}E_k \quad 1$$

$$D_i = e_{ikl}S_{kl} + \varepsilon_{ik}E_k \quad 2$$

Where,

$T_{ij}$  = stresses

$S_{kl}$  = strains

$E_k$  = electric field

$D_i$  = electrical displacement

$C_{ijkl}$  = Constitutive relationship

$e_{kij}$  = piezoelectric coefficient

$\varepsilon_{ik}$  = clamped permittivity

### **Carbon nanotube and nanofibers**

Piezoelectric materials are solid-state smart materials. The limitations of the solid-state materials are tolerance of high voltage, brittleness, and a small range of tolerance of strain and stress. Smart nanoscale materials help to enhance these material properties and represent a new way to generate and measure the motion of the device. Among the various nanoscale materials, carbon nanotubes (CNTs) exhibit mechanical properties that help to improve strain, durability and energy output of piezoelectric material (Kang, et al., 2006). For instance, CNTs are the strongest and most flexible molecular material known due to the unique C–C covalent bonding and seamless hexagonal network (Kang, et al., 2006). The nanotubes also have electrical conductivity or semi-conductivity and high thermal conductivity in the axial direction. The discovery of Multi-Wall Carbon Nanotubes (MWNTs) and the C60 fullerene and single-wall carbon nanotubes (SWNTs) opened the possibility for a new class of smart materials based on

nanoscale materials (Kang, et al., 2006). Structural and electrical characteristics of CNTs make them potential for developing unique and revolutionary smart composite materials. The nanotube continuous strain sensor or the neuron discussed are new approaches to monitor strains and crack propagation in large structures, such as aircraft, helicopters, and civil infrastructures. The power generation property of carbon nanotubes and nanofibers was demonstrated on a vibrating structure, and later, an electrolytically gated carbon nanofiber field-effect sensor was developed for biosensing applications (Kang, et al., 2006).

### Modeling

In order to model an electricity energy harvester, we want to grasp the piezoelectric through effect and strain–charge relationships through the use of the derived equations (Ilyas, 2018):

$$S = [s^E]T + [d^t]E \quad 3$$

$$D = [d]T + [\epsilon^t]E \quad 4$$

Where,

D = electrical displacement of charge

E = force field strength

S = Mechanical strain

T = mechanical stress

$\epsilon^t$  = permittivity of fabric underneath a constant stress

$S^E$  = compliance underneath a relentless electric field

d = matrix for direct electricity

$d^t$  = matrix for reverse electricity effect

t = denotes the matrix operation

E and D are outlined as electrical quantities with vector nature, whereas T and S are mechanical quantities with tensor nature of six elements. The constants in every electricity material referred to as direct electricity, and permittivity of fabric rely upon the directions of an electrical field, displacement, and stress and strain.

In 3 dimensions, the electricity is given by:

$$\begin{bmatrix} D_1 \\ D_2 \\ D_3 \end{bmatrix} = \begin{bmatrix} 0 & 0 & 0 & 0 & d_{15} & 0 \\ 0 & 0 & 0 & d_{24} & 0 & 0 \\ d_{31} & d_{32} & d_{33} & 0 & 0 & 0 \end{bmatrix} \begin{bmatrix} T_1 \\ T_2 \\ T_3 \\ T_4 \\ T_5 \\ T_6 \end{bmatrix} + \begin{bmatrix} \epsilon_{11} & 0 & 0 \\ 0 & \epsilon_{22} & 0 \\ 0 & 0 & \epsilon_{33} \end{bmatrix} \begin{bmatrix} E_1 \\ E_2 \\ E_3 \end{bmatrix} \quad 5$$

For direct piezoelectricity, we tend to use equations to deduce the following co-efficient:

$$d_{ij} = \left( \frac{\partial D_i}{\partial T_j} \right) E = \left( \frac{\partial S_i}{\partial E_j} \right) \quad 6$$

$$e_{ij} = \left( \frac{\partial D_i}{\partial S_j} \right) E = \left( \frac{\partial T_i}{\partial E_j} \right) S \quad 7$$

The energy in an exceeding electricity material is designed as energy stored in an exceeding condenser. Thus, the subsequent equation is derived:

$$W_{33} = \frac{1}{2} Q_{33} V_{33} \quad 8$$

Where  $Q_{33}$  and  $V_{33}$  are described as:

$$Q_{33} = d_{33} F_3 \quad 9$$

$$V_{33} = \frac{T}{WL} F_3 g_{33} \quad 10$$

Where T = thickness

W = width

$L$  = length

$F$  = force

$g_{33}$  and  $d_{33}$  are constants piezoelectric material

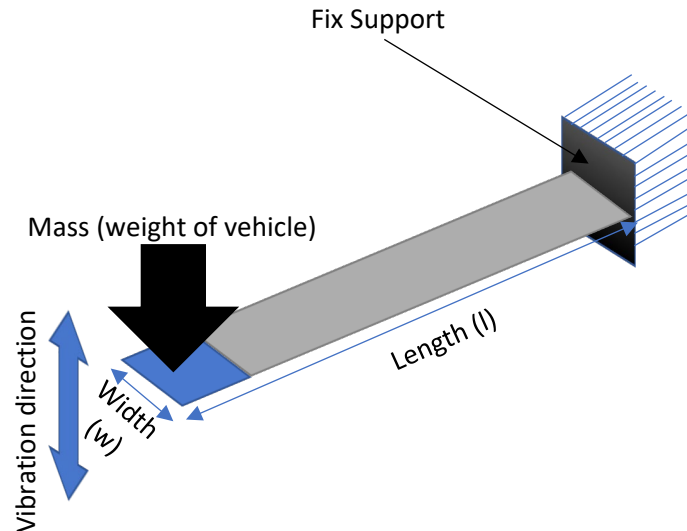


Figure 2 Cantilever arrangement with mass (Andriopoulou, 2012)

### Conceptual Design of the Piezoelectric material in the pavement

Asphalt pavements throughout their lifespan endure repeated loading that causes stress, strain, deformation, and vibration. At the same time, the pavement obtains strain and kinetic energies from the work of carload and gravity as shown in Figure 2 (Andriopoulou, 2012). Electricity transducers embedded into the pavements also have the potential to harvest the waste energy and store it within the electronic capacitance. To date, the harvested energy has been used for small scale road applications like road furnishings, lighting, edge advertising or railway and aerodrome assemblage wherever the installation and maintenance price is practical (Jasim et al., 2017).

Figure 3 shows the schematic design of an array arrangement of piezoelectric transducers under the pavement. This arrangement will be used for the numerical analysis in chapter 4. The number of columns and rows of the piezoelectric transducers depend on the number of transducers that needs to be placed.

Number of transducers also affect the efficiency of the power output.

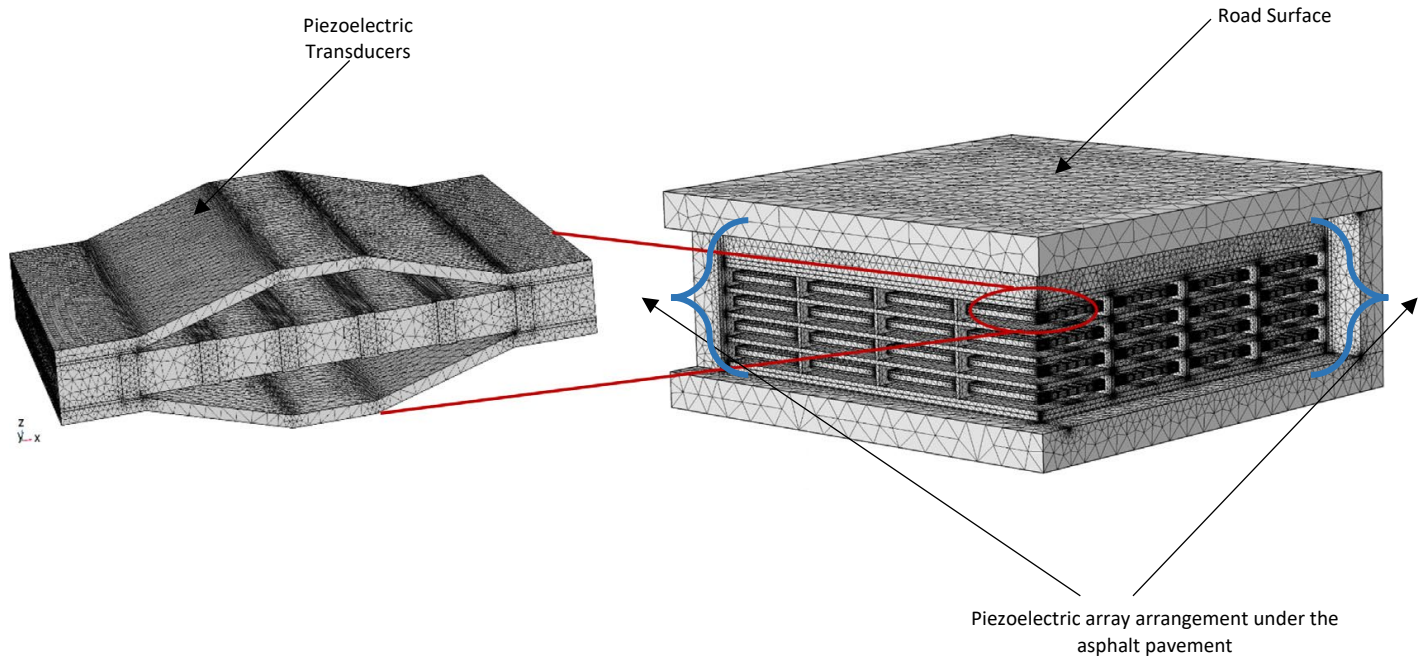


*Figure 3 Schematic of piezoelectric transducers embedded in a pavement (Jasim, et al., 2018)*

Jasim et al. (2018) tried to judge the potency of the sensing element by use of its potential electrical output and its coupling effects with the pavement (pavement's displacement). Therefore, increasing both the diameter and the thickness of the PZT and the thickness of the cap steel, the mechanical energy is increased beside the value (Jasim et al., 2017). There are two types of structural design of piezoelectric transducer, Moonie structure and Cymbal. However, the Cymbal structure looks like bridge structure but the structural loading condition in both is different from each other as shown in Figure 5 and Figure 6 (Zhao, Ling, & Yu, 2012).

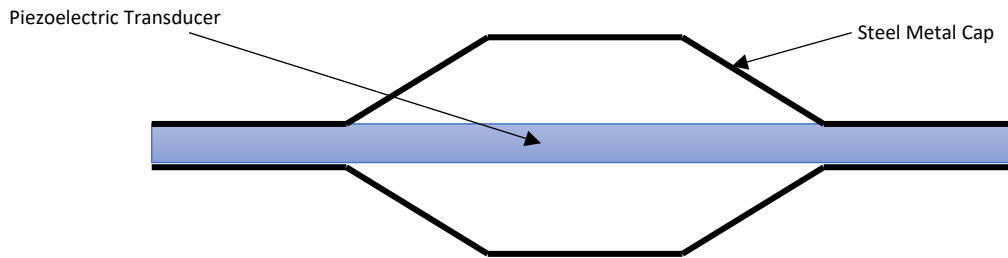


Figure 4 Schematic layout of the PZT transducer (Jasim, Wang, Yesner, Safari, & Maher, 2017)

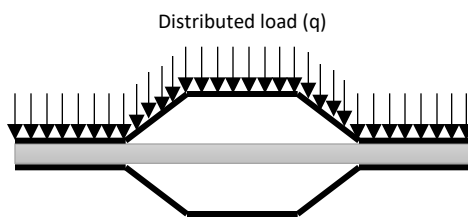


Figure 5 Loading condition in Cymbal piezoelectric transducers (Zhao, Ling, & Yu, 2012)

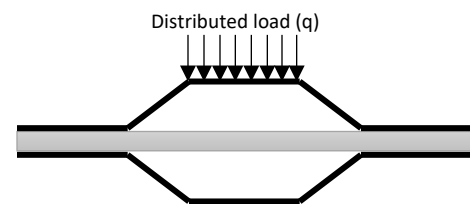


Figure 6 Loading condition in Bridge piezoelectric transducer (Zhao, Ling, & Yu, 2012)

### Factors affecting the performance of energy harvester

The following factors have to be considered during the designing steps for the piezoelectric material as well as in deciding the location of the piezoelectric transducer under the pavement; overall these factors affect the efficiency of the output of electricity of the piezoelectric transducers.

1. Effect of epoxy thickness on transducer failure
2. Effect of gap design on energy harvester performance
3. Effect of cover/gap material on energy harvester performance

### Simplified Design for the piezoelectric transducer

It had been found that the synthetic PZT-5H part was applicable in pavements because it exhibits the highest electricity property from 25° to 170° (Najini & Muthukumaraswamy, 2016). Higher electricity property is well inside the Curie temperature (at a certain temperature the material tends to lose its permanent magnetism). It was tested that the design of electricity transducers from the study given would surrender to 150kW/h per lane per

click (Zhao et al., 2012). According to the results of Najini and Muthukumaraswamy (2016), it is confirmed that the PZT piles and multilayer, cycloidal plates of brasses, that create the electrical device to bridge the piles along, have the potential of operating underneath the asphalt pavement atmosphere. It had been suggested to use 8-16 PZT piles for pavement space wherever these PZT piles were organized between the circular steel plates as seen in Figure 7.

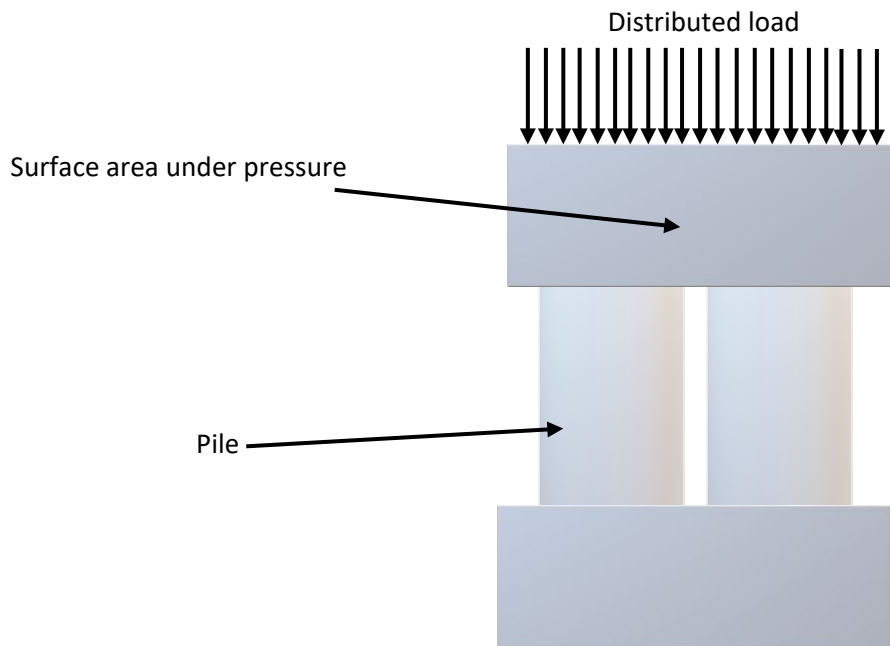


*Figure 7 Structure of Piezoelectric Transducer (Zhao et al., 2014)*

The form of the PZT piles was to make sure of the reduction of stress concentration in an area, whereas the multi-layering was suggested to decrease the electrical potential of the generator. Moreover, multiple references describe these generators work as sensors that are inside the pavement to observe the traffic movement, pavement stress, and condition.

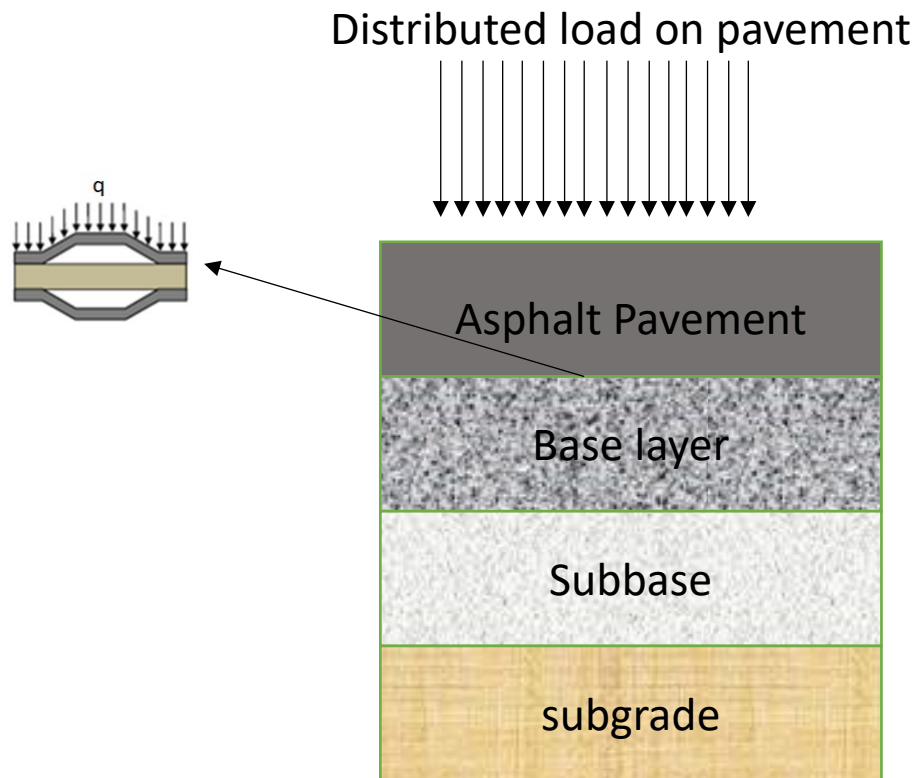


Figure 8 Location of a piezoelectric transducer (Najini & Muthukumaraswamy, 2016)

The piezoelectric transducers are embedded under the asphalt pavement to produce the electricity from the kinetic energy to electric energy. As shown in Figure 8, the location of piezoelectric transducers is immediately below the asphalt layer and the depth of asphalt layer is approximately 3-5 inches. In this design of piezoelectric, the pile structure is used and that can produce 50 kWh from the pavement under significant traffic conditions (Najini & Muthukumaraswamy, 2016).

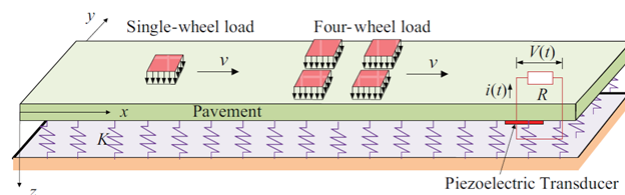


Figure 9 Plate on elastic foundation subjected to moving distributed loads (Zhang, Xiang, & Shi, 2016)

## Wind turbine

Wind energy is another common approach to harvest the energy. This section describes the past few papers on the application of the wind turbine along the highway side. Hu et al. (2018) wrote the paper on the application of Vertical Axis Wind Turbine (VAWT) along the highway side, which explained the determination and utilization of the wind characteristics, flow field, and principle. In that paper, the finite element method has been used to calculate the electricity output. The concept of this paper is similar to that paper, but in that paper VAWT turbine is used. The helical wind turbine is more efficient than the VAWT (Tong, 2010). The explanation about the helical wind turbine is covered later in this chapter.

There was another paper that explained about the application of S-rotor and H-rotor turbines at the high-speed railway tunnels (Pan, et al., 2019), which proposed the wind energy harvesting method inside the tunnel to fulfill the need of the electricity inside the tunnels. Pan et al. (2019) developed self-powered application of wind turbines for the tunnels. There are three main components: harvesting mechanism, main module (Converter), and power storage module. The analysis of the output in the Pan et al. paper is carried out with finite element method (FEM). This paper is important for the comparison of result of FEM and MATLAB simulation and location.

In addition, Wind energy technology recognizes the technical complexity and deployment speed of wind power and the fact that the percentage of wind integrated into the electricity system cannot be limited in practical terms. It has been estimated that the total solar energy received by the earth is approximately  $1.8 \times 10^{11}$  MW. Of this solar energy input, only 2% is converted into wind energy and around 35% of wind energy is dissipated within 1000m of the earth's surface (Tong, 2010). Therefore, the available wind power that can be converted into other forms of energy is approximately  $1.26 \times 10^9$  MW. Since this value represents 20 times the rate of the present global energy consumption, wind energy in principle could meet all the energy needs of the world (Tong, 2010).

Recently, there have been three types of modern vertical axis wind turbines (VAWT) according to their blade design. The designs which are useful to harvest energy efficiently are the Savonius turbine, Darrieus turbine, and H-rotor. Different designs of a wind turbine have different efficiency and characteristics which affects the output of electricity generation.

### **Darrieus turbine**

There is a considerable amount of research going on relating to VAWTs as varied universities and research establishments have allotted in-depth analysis activities and developed varied styles based on many mechanics' models. These models are crucial for deducing optimum style parameters and additionally, they predict the performance before fabricating the VAWT (Mazharul et al., 2006). In this review, the authors have compiled the mechanical models that are used for performance prediction and style of straight-bladed Darrieus-type VAWT as shown in Figure 10. At this time, it has been discovered that the foremost widely used models are double-multiple stream tube model, the Vortex model, and the Cascade model. These are the modified design of the VAWT for more power output. It is important to compare to decide the optimal design of the VAWT.

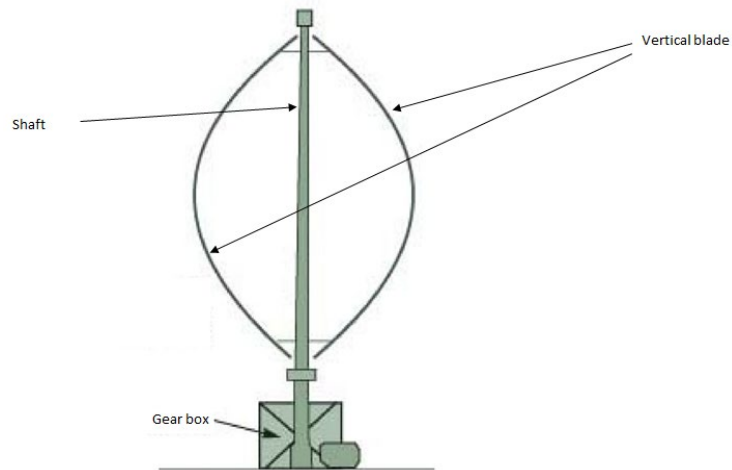


*Figure 10 Curved blade Darrieus VAWT (Tong, 2010)*

### **Savonius wind turbine**

S.J. Savonius invented this type of VAWT turbine in 1925 (Tong, 2010). It is primarily a drag force driven turbine with two cups or half drums mounted to a central shaft in opposing directions. Every cup/drum catches the wind and so turns the shaft, delivering the opposing cup/drum into the flow of the wind as shown in Figure 11. This cup/drum then repeats the method, inflicting the shaft to rotate more, therefore finishing a full rotation. This method continues when the wind blows all the time; the rotating shaft is used to drive a pump or a small generator. This type of rotary engine is appropriate for low-power applications and the area units are typically used for wind speed instruments (Tong, 2010).

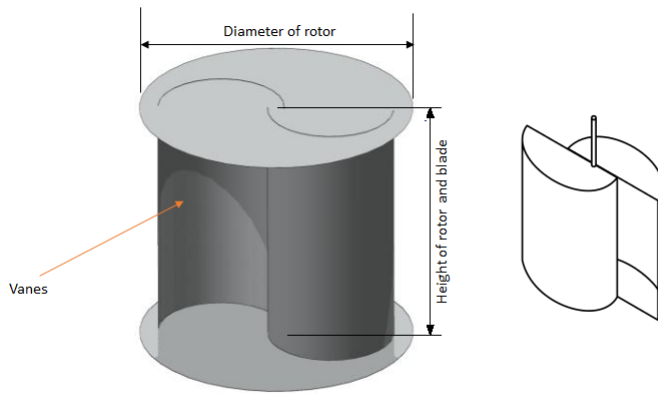


Figure 11 Savonius type VAWT (Tong, 2010)

## H-rotor

H-Rotors, as shown in Figure 12, were developed within the United Kingdom through the analysis carried out throughout the 1970–1980s (Tong, 2010). Once it was established that the elaborate mechanisms would not feather, the straight-bladed Darrieus VAWT blades were superfluous. It was distinguished that through the drag/stall result created by a blade effort the wind flow would limit the speed that the opposing blade (in the wind flow) might propel the entire blade configuration forward.

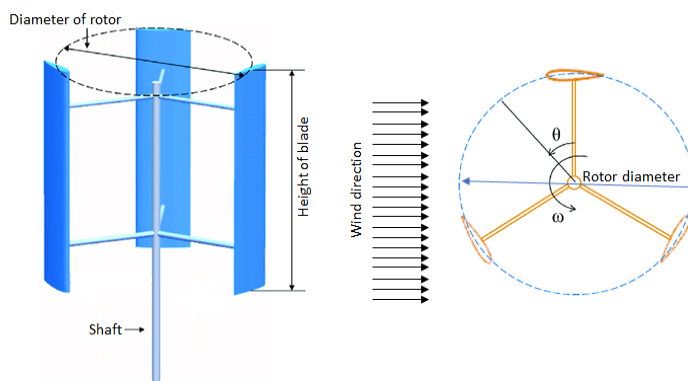


Figure 12 H-rotor type VAWT

## **Solar Energy**

Solar energy is electric or thermal energy that is converted from the sun. Solar energy is the cleanest and most abundant renewable energy source available, and the United States (U.S.) has some of the richest solar resources in the world (Andriopoulou, 2012). There are three different ways through which solar energy can be harvested: photovoltaics, solar heating and cooling, and concentrated solar power. It has been estimated that the total solar power received by the earth is approximately  $1.8 \times 10^{11}$  MW (Andriopoulou, 2012). This thesis paper does not include the analysis on the solar roadways due to many practical applications yet to be overcome; however, it can be used for future reference.

## **Wireless Charging Technology**

Wireless charging technology is based on the principle of inductive coupling (Bansal, 2015). In this kind of coupling, a circular magnetic field is generated as a result of the movement of current through a wire coil. If another loop of the coil is placed close to the first coil, a current will be induced in it. The concept of inductive charging has been used for charging small electronic devices like toothbrushes, cellphones, and tablets with power mats acting as the primary coil. Mutual inductance occurs when the change in current in one inductor induces a voltage in another nearby inductor (Bansal, 2015). The mechanism of wireless charger is like transformers, but it can also cause unwanted coupling between conductors in a circuit. In wireless charging technology, an induction coil present in the induction chargers creates an electromagnetic field within a charging base station. Another induction coil in the small transformers acquires the energy generated due to the electromagnetic field and converts it into electric current for charging the battery. These coils are regulated to have the same resonant frequency in order to avoid energy leakage and reduce the risk of electrical shock.

## **Qualcomm HALO WEVC (Wireless Electric Vehicle Charging)**

Wireless Electric Vehicle Charging (WEVC) technology operates on the principles of magnetic inductance and magnetic resonance. Similar to the way a transformer operates, a magnetic field is induced in the surrounding area by running currents through a coil of wire. Exposing another coil nearby to that magnetic field will induce an electric current in the nearby coil; thus, wireless power transfer (WPT) is achieved (Bansal, 2015). However, unless the coils are very close together and aligned correctly, this power transfer method, known as inductive power transfer, typically has a suboptimal efficiency.

### **Level of charging**

Based on the EV charging installation guide, these are the following levels for charging as provided by Bansal (2015):

Level 1: 120 V AC.

This is a common charger, which is used for residential charging purposes. The current rating for this case is in the range of 15 A – 20 A.

Level 2: 240 V AC.

These are used for the public charging facilities. The main reason is their efficiency in charging as compared to level 1 charging. They use 220-240 V range and current is of the order 80-100 A.

Level 3: DC Fast Charging.

This type of charger would provide a fast recharge and fifty percent of the total recharge in just 10-15 minutes. It is suitable for the vehicles' on-board battery management system that controls the off-board charger to deliver the direct current (DC) to the battery.

### CHAPTER 3 OVERVIEW ABOUT LOCATION

The main aim of this study is to analyze the 3<sup>rd</sup> avenue of Huntington, WV from 20<sup>th</sup> street to Hal Greer Blvd (Figure 13). According to the traffic record of 2018, the daily average traffic on this avenue is 14732, and during the peak hour, the traffic count is 1264. According to the Federal Highway Administration’s data, the annual average mean air temperature in a specific location is 12 °C (FHWA, 2019). The results about how much electricity can be produced from piezoelectric and wind sources from that specific section within 24 hours have been carried out. Moreover, the comparison of output from harvesting source with the average daily requirement of the Marshall University Weisberg Applied Engineering Complex will be presented. The calculation has been carried out with the help of the MATLAB coding for the strain, energy output from piezoelectric transducers and wind turbine; MATLAB code is given in appendix B, C and D.

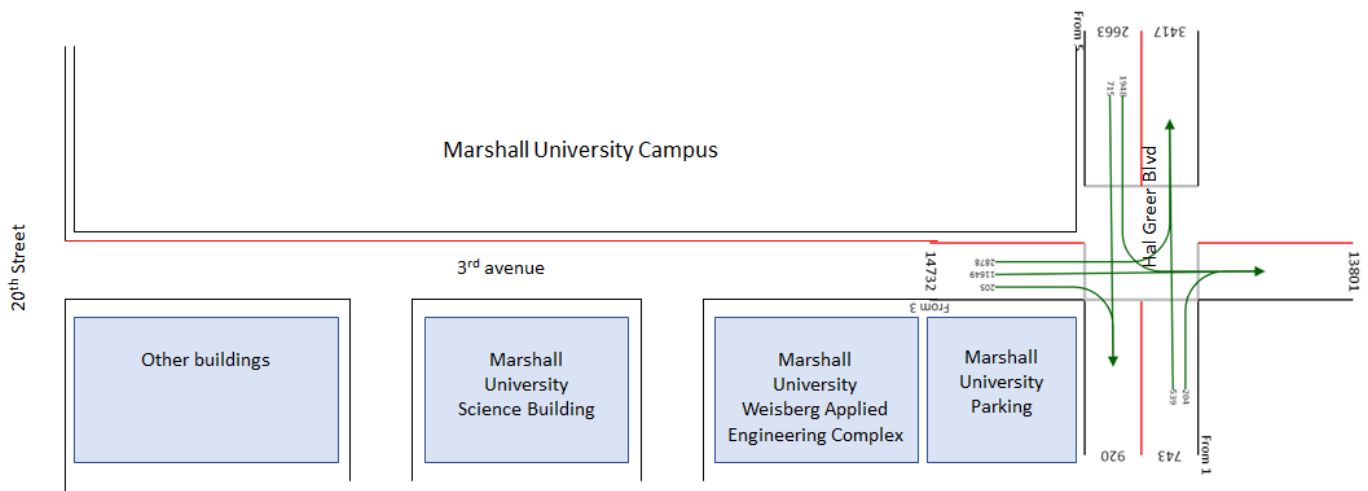


Figure 13 Intersection of 3rd avenue and Hal Greer Blvd

## CHAPTER 4 NUMERICAL ANALYSIS

### Piezoelectric material

This section covers the explanation of the methodology to calculate the conversion of the kinetic energy to electric energy. The main principle is kinematic displacement of pavement and the output depends on speed, load intensity of the vehicle, strain, and structure of the pavement. The FEM and numerical simulation are two approaches for the calculation of power output. In this paper, the latter approach is used, and the MATLAB code is given in appendix B. Also, the MATLAB code for an empirical analysis is given in appendix C; this analysis is detailed later in this chapter.

### Formulas for the piezoelectric material

This section includes the important formulas that help to design, calculate and analyze the output of piezoelectric transducers under the pavements. In this section, Table 1 gives the values of constants for the piezoelectric calculation.

#### Capacitance

Capacitance can be defined as the capacity of piezoelectric transducers to store the electricity generated by the dynamic impact load and using by equation 11.

$$C_s = \frac{K_{33}^T E_0 l w}{h} \quad 11$$

Where,  $C_s$  = Capacitance

$K^T$  = relative dielectric constant (constant stress)

$E_0$  = permittivity of free space ( $8.85 \times 10^{-12}$  farad/m)

$l$  = length of ceramic element (m)

$w$  = width of ceramic element (m)

$h$  = height (thickness) of the ceramic element (m)

Static displacement

Static displacement is the amount of cymbal PZT compresses under the distributed load equation

$$\Delta h = d_{33}V \quad 12$$

Where,  $\Delta h$  = Vertical displacement

$d_{33}$  = Piezoelectric charge constant (C / N)

V = Voltage

Static Voltage

Static voltage is the potential difference between the positive and negative pole. The electric charges move because of the potential difference between the two nodes equation 13.

$$V = \frac{g_{33} F_3 h}{l w} \quad 13$$

Where, V = Voltage

$g_{33}$  = Piezoelectric voltage constant

$F_3$  = Force

l = length of ceramic element (m)

w = width of ceramic element (m)

h = height (thickness) of the ceramic element (m)

Table 1 Piezoelectric Constant (Jasim, Wang, Yesner, Safari, & Maher, 2017)

Material Properties	Symbol	PZT Material Type						
		4	4D	5A	5H	5J	8	5X
Piezoelectric Charge Constant (pC/N)	D <sub>33</sub>	289	320	374	593	530	225	750
	D <sub>31</sub>	-23	-45	-171	-274	-230	-37	-320
Piezoelectric Voltage Constant (x10 <sup>-3</sup> Vm/N)	G <sub>33</sub>	26.1	26.7	24.8	19.7	22.6	25.4	19
	G <sub>31</sub>	11.4	-11.8	-11.4	-9.11	-9.8	-10.9	-8.2
Relative Dielectric Constant	ε <sub>33</sub>	1300	1450	1700	3400	2600	1000	4500
	ε <sub>31</sub>	1475	1610	1730	3130	2720	1290	4410
Poison's Ratio	q <sup>E</sup>	0.33	0.35	0.35	0.34	0.35	0.33	0.35
Elastic Modulus (10 <sup>10</sup> N/m <sup>2</sup> )	γ <sup>E</sup>	8	7.5	7.4	6	6.8	8.6	6.1
Density (Kg/m <sup>3</sup> )	ρ	7500	7600	7750	7500	7400	7600	7400
Elastic Compliance at Constant Electric Field (10 <sup>-12</sup> m <sup>2</sup> /newton)	S <sup>E</sup> <sub>11,22</sub>	12.3	13.3	16.4	16.5	16.2	11.5	16.4
	S <sup>E</sup> <sub>12,21</sub>	-4.05	-4.76	-5.74	-4.78	-4.54	-3.70	-4.78
	S <sup>E</sup> <sub>32,31,23,13</sub>	-5.31	-7.22	-7.22	-8.45	-5.9	-4.80	-8.45
	S <sup>E</sup> <sub>33</sub>	15.5	-6.2	18.8	20.7	22.7	13.5	23.3
	S <sup>E</sup> <sub>44,55</sub>	39	16.8	47.5	43.5	47	31.9	43.5
	S <sup>E</sup> <sub>66</sub>	32.7	42	44.3	42.6	41.5	30.4	42.6
			36.1					

## Formulation

The initial analysis of what kind of piezoelectric material is appropriate for this implementation was detailed within an earlier section of this thesis. Considering the assorted piezoelectric parts that exist, it had been found by Najini and Muthukumaraswamy (2016) that the PZT-5H was the foremost acceptable material on coming up with an energy harvest style system for the appliance of generating energy from the moving traffic and the road.

This form of implementation was achieved by fixing the empirical structure of the pavement such that it behaved as a sort of a plate resting on the Winkler foundation. This technique was mentioned in that it deals with the classic plate theory based on Kirchhoff-Love's plate theory and Navies answer in conjunction with Fourier analysis, Cauchy's residue theorem, and then on (Zhang et al., 2016). To deduce the deformation of the pavement, the governing equation of the pavement is denoted by equation 14 that was obtained consistent with Kirchhoff-Love's plate theory, or called the classical plate theory (Reddy, 2006).

$$D\nabla^4\omega(x, y, t) + \rho h \frac{\partial\omega(x, y, t)}{\partial t^2} + K\omega(x, y, t) = F(x, y, t) \quad 14$$

Where,

K = modulus of the subgrade reaction

$\rho$  = density

t = time

The flexural rigidity of the pavement D is given by

$$D = \frac{Eh^3}{12(1 - \mu)} \quad 15$$

Where,

E = Young's modulus

$\mu$  = Poisson's ratio

h = thickness of the pavement

The fourth-order displacement gradient is addressed by the following equation with the Winkler foundation represented by the second and the third term of Equation 16.

$$\nabla^4\omega(x, y, t) = \left[ \frac{\partial\omega^4(x, y, t)}{\partial x^4} + 2\frac{\partial\omega^4(x, y, t)}{\partial x^2y^2} + \frac{\partial\omega^4(x, y, t)}{\partial y^4} \right] \quad 16$$

Incorporating Equation 14 and 16 in the piezoelectric equation given by equation 17 estimates the power produced in each piezoelectric transducer unit (Zhao et al., 2012).

$$C_0 \frac{dV(t)}{dt} + \frac{V(t)}{R} = \frac{dQ(t)}{dt} \quad 17$$

Moreover, this form of implementation is advantageous than the bimorph (cantilever) structural implementation for the following reasons:

- The output power increases with the decrease in the condition of the road structure, and
- The output power increases with the decrease in smaller bridges span length

The total power generation estimation is required because the power loss analysis is dynamic. The main reason for the dynamic loss of generated power is the component of a system like DC boost converter, rectifier, and inverter (Najini & Muthukumaraswamy, 2017). The main limitation of this kind of system is that it may not be able to capture all kinetic energy and convert into useful energy because of the heat loss and the high-speed of vehicles. To estimate the utilized kinetic energy that is produced by the vehicles which are traveling at a different velocity and the moving load is continuously applying on the pavement is known as load intensity which is given by equation 18 (Najini & Muthukumaraswamy, 2017).

$$\begin{aligned} & \text{Load Intensity} \\ & = \frac{\text{Mass of vehicle (N)} * \text{coefficient of rolling friction} * \text{Contact tires}}{\text{area of contact}(m^2) * \text{speed of travel}(\frac{\text{mile}}{\text{hour}})} \quad 18 \end{aligned}$$

## Results

The results are carried out based on the actual traffic data for typical hours and peak hours from FHWA, and constant based on the material properties. The load of a vehicle per axle is 3300 N. The piezoelectric transducers are provided under the wheel load on each side of the vehicle. There are two sets of piezoelectric material that are considered – those on the left side of the car (left wheel load), and those

on the right side of the car (right wheel load). Individually, the left and right wheel load piezoelectric materials are in series connection. However, if one considers both the left and right wheel load piezoelectric material chains for the entire lane, they are in parallel connection. Kirchhoff-Love's Plate Theory can be used if the width and thickness ratio of the piezoelectric plate was equal to 7. There are two different results included: Winkler's foundation equation and empirical strain equations detailed in Bryce et al. (2019). The results of the two approaches are compared in order to better understand the influence of strains on energy output.

In this section, Table 2 gives the specification of the piezoelectric transducers which are going to be used for the analysis. Table 3 gives the physical dimensions of the transducers. Table 4 and Table 5 explain the output of electricity from 33000 cymbals piezoelectric material during typical hours and peak hour respectively. The estimation of number of piezoelectric materials depends on the dimensions of transducers, area of the road, and the location of the piezoelectric from the top surface.

*Table 2 Piezoelectric Transducer Specifications*

<b>Parameter</b>	<b>Value</b>
<b>Poisson's Ratio</b>	0.15
<b>Young's Modulus E (Mpa)</b>	27560
<b>Winkler Modulus (N/m)</b>	136 <sup>b</sup> .
<b>Resistive Load (N)</b>	800
<b>Mass of Vehicle (N)</b>	3200 <sup>a</sup> .
<b>Coefficient of Rolling Friction</b>	0.015
<b>Contact Tires</b>	2
<b>Area of Contact (m<sup>2</sup>)</b>	0.0025
<b>Speed of Travel (mile/hr)</b>	35-45

a. Mass of vehicle is higher due to the location of a steel factory close to the road evaluated.

b. Winkler modulus is obtained from Najini and Muthukumaraswamy (2017).

Table 3 Piezoelectric Transducer Dimensions

Parameter	Dimension (m)
Length	0.14
Width	0.14
Depth	0.02

All the calculations have been performed under Winkler’s foundation equation and the equation from Bryce et al. (2019). For the Bryce et al. (2019) approach which is specific to strains in asphalt pavements, I referred the equation which is described in Bryce et al. (2019) for better accuracy to get the strain value. From Table 4, the values for the strain at the various locations underneath the pavement surface are reasonable based on Bryce et al. (2019). The strain is effective factor for the power out through piezoelectric material that can be defined from difference in output. In Table 5 and Table 6, the results are shown for both approaches. Table 5 is the result for the typical traffic hours and the result in Table 6 is based on the peak hour traffic count.

Table 4 Strain Values for the Asphalt Pavement

Strain Values for Different Levels of the Asphalt Pavement						
Speed Limit (mile/hr)	Assumed Asphalt Layer Thickness (m)	Assumed Base Thickness (m)	Horizontal Bottom HMA	Vertical Mid HMA	Vertical Top Subgrade	Vertical Mid Base
30	0.2032	0.2540	$1.27 \times 10^{-4}$	$6.30 \times 10^{-5}$	$5.18 \times 10^{-5}$	$2.34 \times 10^{-4}$
35	0.1524	0.2032	$1.62 \times 10^{-4}$	$6.15 \times 10^{-5}$	$7.65 \times 10^{-5}$	$3.23 \times 10^{-4}$
40	0.2540	0.1524	$1.11 \times 10^{-4}$	$6.72 \times 10^{-5}$	$3.34 \times 10^{-5}$	$2.39 \times 10^{-4}$

Table 5 Power estimation from 20th Street to Hal Greer Blvd (0.5 miles)

	<b>Winkler's Foundation Method</b>	<b>Bryce et al. (2019)</b>
<b>Number of Transducers</b>	33000	33000
<b>Hourly Traffic Rate</b>	620	620
<b>Speed Limit (mile/hr)</b>	30	30
<b>Total Power (piezo/mile/hr)</b>	70.50	70.50
<b>Total Power (kWhr)</b>	230.169	250.230

Table 6 Power estimation for Peak Hour

	<b>Winkler's Foundation Method</b>	<b>Bryce et al. (2019)</b>
<b>Number of Transducers</b>	33000	33000
<b>Hourly Traffic Rate</b>	1200	1200
<b>Speed Limit (mile/hr)</b>	30	30
<b>Total Power (piezo/mile/hr)</b>	139.70	139.70
<b>Total Power (Wmin)</b>	7523	7523
<b>Total Power (kWhr)</b>	455.60	478.23

### Cost analysis

An estimation of the costs has also been conducted to support the information calculated from the previous section. This paper considers all the conditions which are described in Chapter 2 for the Levelized cost of the piezoelectric cymbals per energy generated by the embedded piezoelectric cymbals in our specific conditions. The line in Figure 14 marks the value calculated for the present technology shown during this work. The blue line indicates the calculation for an additional price reduction of 90% because it saves additional land lease cost and addition power unit cost (Moure, et al., 2016). The three regions correspond to the bounds of the \$64000 current prices for standard, photovoltaic sources and windmill technologies, respectively.

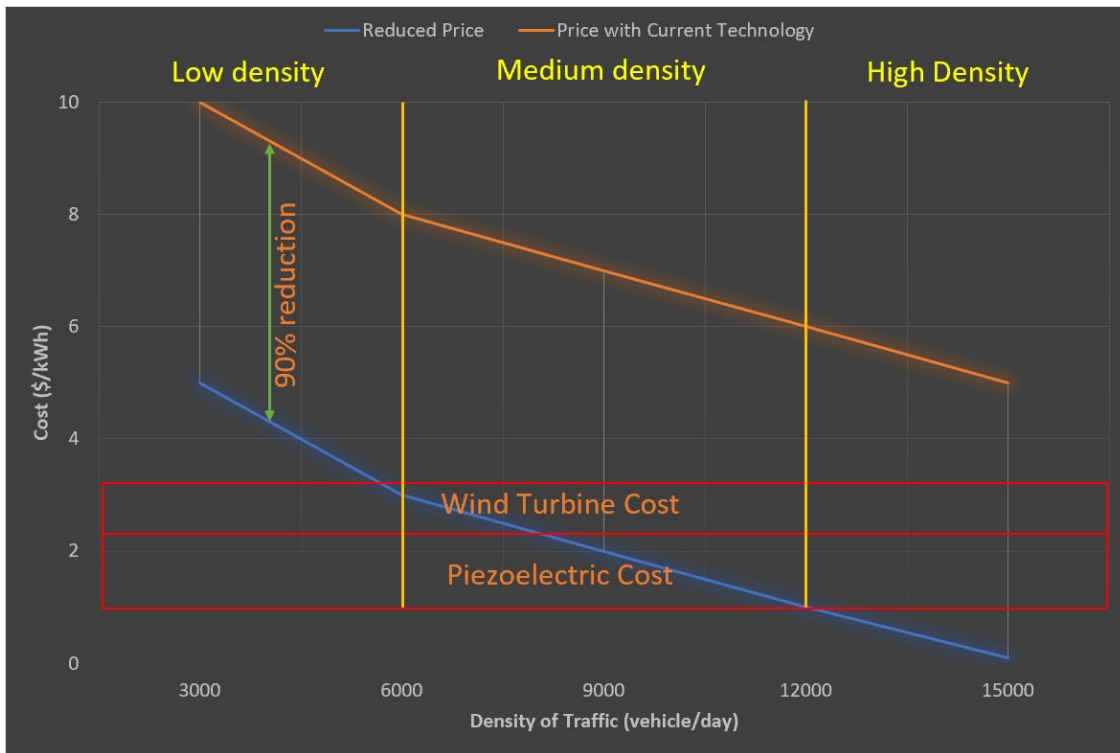


Figure 14 Cost as a function of the vehicle density (Guo & Lu, 2017)

The effective cost estimation is not only relying on the electricity generated from the pavement. In this section, the potential benefits are evaluated based on the investment cost per each unit over their lifetime. The effective cost analysis can be defined as a Levelized cost of electricity, which is as follows (Guo & Lu, 2017):

$$LCOE = \frac{\text{sum of cost over lifetime}}{\text{sum of electricity produced over lifetime}} \quad 19$$

$$LCOE = \frac{C_p + C_i}{W_p N w 365 Y} \quad 20$$

Where,  $C_p$  = cost of each PZT unit (\$)

$C_i$  = cost of installation (\$)

$W_p$  = energy output from each PZT unit per vehicle (kWh)

$N$  = number of vehicles per day

$w$  = equivalent hit rate (frequency of air impact on the blades)

$Y$  = service life (year)

The normal rate for the cymbal piezoelectric transducers per meter square is \$1000, and the installation cost is \$50/m<sup>2</sup> (Guo & Lu, 2017). Here, the dimension of the road is 804 m x 12 m. So, the total cost of a cymbal piezoelectric transducer for the specific area is \$1.01 million. The total cost for each cymbal is \$306. The average number of vehicles per day is 22,000. The expected life span is 15 years.

*Table 7 Levelized cost for the piezoelectric material*

<b>33000 Cymbals Transducers in 0.5 miles</b>	
<b>Estimated Cost (<math>C_p + C_i</math>) (\$ in millions)</b>	1.01
<b>Energy Output (<math>W_p</math>) (kWh/vehicle)</b>	0.0109
<b>Number of Vehicles (per day)</b>	14732
<b>Equivalent Hit Rate</b>	100
<b>Expected Service Life (years)</b>	15
<b>Levelized Cost (\$/kWh)</b>	$2.44 \times 10^{-4}$

## Wind Turbine

This section includes the explanation of the conceptual design of the helical wind turbine set up along the highway. However, that design cannot be used due to certain limitations which are explained in upcoming sections. The proposed design section explains the solution for that limitation. In this section, analysis for the power output and cost estimation for power generation are also covered.

### Conceptual Design of the wind turbine along the highway

In the literature review, proposal design is shown in Figure 15, which has few drawbacks that are not good for road users. The specific design shown in Figure 15 did not appear as environmentally friendly due to the large propellers, which can be dangerous for the local birds and wildlife. In this design, wind turbines placed into road dividers or on overhead poles as seen in the design (Champagnie, Altenor, & Simonis, 2013). Champagnie et al. (2013) calculated that with cars moving at 70 mile/hr, 9,600 kilowatts of electricity may be produced per annum using the researchers' design in Figure 15.

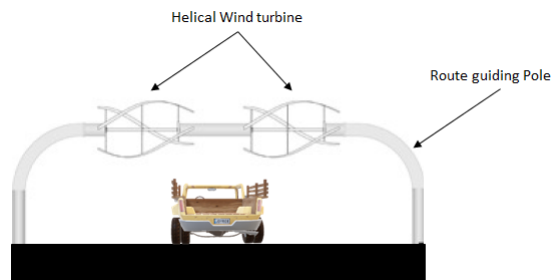


*Figure 15 Cross Section of Road with Wind Turbine (Malave & Bhosale, 2013)*

In Figure 15, the turbines are embraced above the roads. This style is especially complicated as a result of the poles needing to be fitted with vanes so as for the wind made by vehicles to reach the turbines within. This style was not implemented because of safety considerations (Malave & Bhosale, 2013). The components are tiny and might simply be snapped out of place. This style may be rejected because it requires specially designed support posts.

## Proposed Design

Vertical axis wind turbines will be placed on roadways that have a high volume of fast-moving traffic. The electricity generated can then be stored in batteries. Since the electricity made is direct current (DC) it should be converted to electricity (AC) before it is used for lighting the road lamps, sold to the grid or any of the ways in which we tend to use electricity these days (Bani-Hani, et al., 2018) and implies that the DC current should be sent to an electrical converter first before it is used. Figure 16 shows a sample vertical axis turbine with half labels.

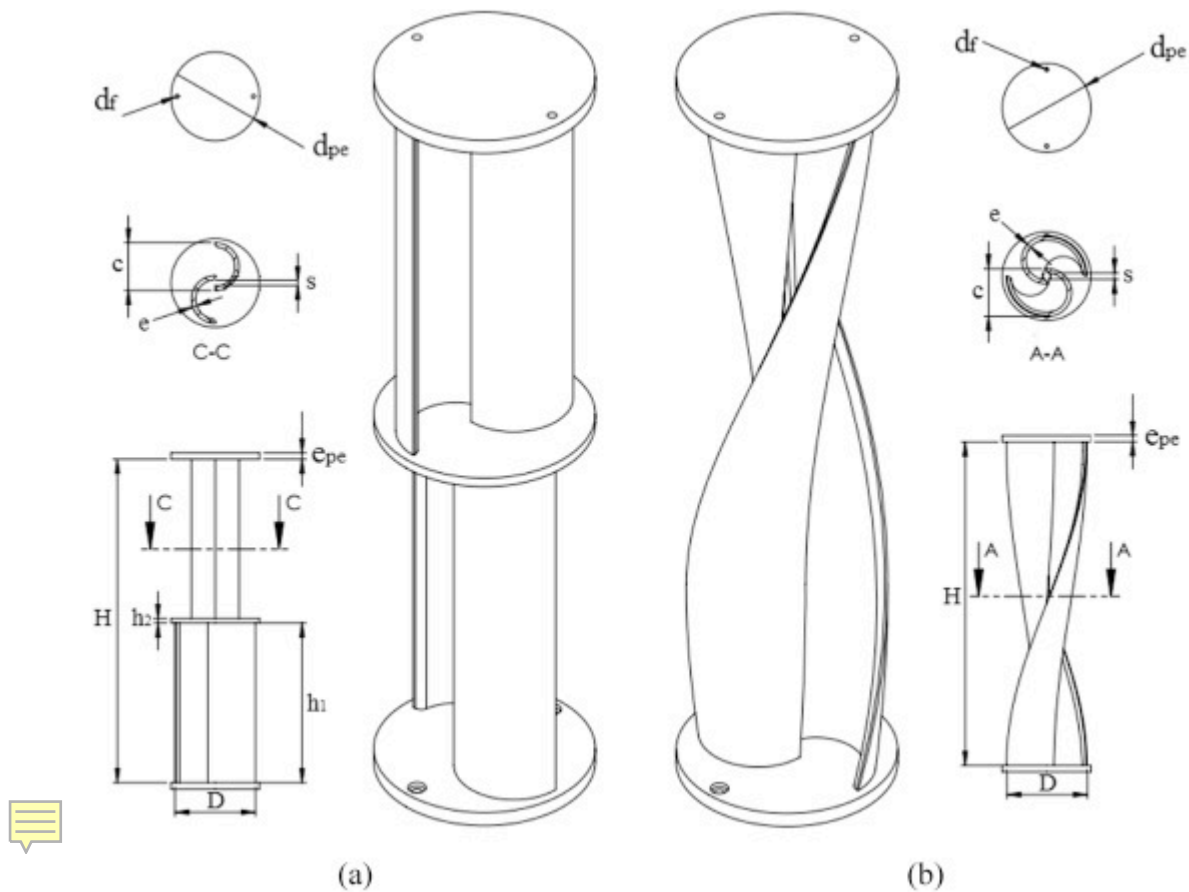


Figure 16 Helical Wind turbine (Kothe, Moller, & Petry, 2019)

## Analytical Analysis

Hu et al. (2018) has done calculation for the VAWT on the expressway with help of FEM. This paper covers the calculation for the helical wind turbine through MATLAB with Monte Carlo's simulation

for accuracy. The formulas that are used to run the simulation to get a power output from wind turbine for every hour of the day is covered later in this section. The MATLAB code for the power output is given in appendix D. The calculation of power output under ideal conditions is also calculated for the comparison with results from the actual data.

The blade area is given by:

The total area of the helical blade for the wind turbine to maintain the ratio of the dimensions of the rotor, shaft, and blade.

$$A = 2 R H \tag{21}$$

Where A = area of the blade (m<sup>2</sup>)

R = rotor radius (m)

H = height of the rotor

The formulas which are helpful to design an efficient turbine are as follows:

$$Power\ available = \frac{1}{2} \rho A V^3 \tag{22}$$

The power coefficient (CP) is the power extracted divided by the power available (Nakil, Tekale, Sambhus, & Patil, 2016).

$$C_p = \frac{Power\ extracted}{\frac{1}{2} \rho A V^3} = \frac{\frac{1}{2} \rho A V^3 \eta C_p}{\frac{1}{2} \rho A V^3} = \frac{P_m}{Power\ available} = \frac{Power\ out}{Power\ in} \tag{23}$$

$$= \eta_b \eta_m \eta_e$$

Where P<sub>m</sub> = (2 π N T / 60)

η<sub>b</sub> = blade aerodynamic efficiency

η<sub>m</sub> = mechanical efficiency

η<sub>e</sub> = electrical efficiency

The maximum value for the power coefficient is called the Betz limit.

$$C_{p \max} = \frac{\frac{8}{27} \rho A V^3}{\frac{1}{2} \rho c^3} = \frac{16}{27} = 0.5926 \quad 24$$

Now the most mechanical power which will be extracted from a given wind stream is outlined by what is referred to as the Betz limit, therefore, the ability extracted is calculated by the following equation (Champagnie et al., 2013).

$$\text{Power extracted} = \frac{1}{2} \rho C_p A V^3 \quad 25$$

Where, V = Wind Velocity

$\rho$  = Fluid Density

These equations show that velocity is the most important factor in generating power. Power is directly proportional to the cubed speed of the wind.

According to the FHWA (2019), the wind speed in Huntington is on average (annually) of 3.5 m/s. Specifically, on 3rd Avenue, the speed limit for the vehicle is 30 mile/hr. So, because of traffic flow and actual average wind speed, the upper limit of the wind speed should be maximum 6 m/s. Mostly, the height of the streetlight pole is 9 feet to 14 feet. Based on height of streetlight pole, the area of the blade does not suppose larger than 1 m<sup>2</sup>. In our specific location, I assumed that 0.950 m<sup>2</sup>. The air density is equal to the standard sea-level value for standardizing value which is 1.225 kg/m<sup>3</sup>. The following calculation is just for the idealized condition of weather, wind, and efficient wind turbine.

Given parameter,

Wind velocity (V) = 6 m/s

R = 0.70 m

H = 1.43 m

From equation 5.1  $A = 2 \text{ m}^2$

$C_p = 0.4$  (Normal efficiency of VAWT)

$\rho = 1.225 \text{ kg/m}^3$

generated power = 114.619 watt

By substituting the value of the given parameter in equation 25, the maximum generated power is 114.619 watt. So theoretically, it can produce 3.5 MWhr electricity per year on the wind speed of 6 m/s. However, we must be concerned about the cost of a wind turbine, design of blades, and materials. According to the previous research, aluminum is the best material for the wings to keep the wind turbine lighter in weight and improve the efficiency because lighter weight can rotate at higher speed. The main disadvantage is the special lighting pole design.

This thesis also investigated the power from wind using hourly wind data. We have done the calculation for the wind turbine power generation through MATLAB distribution as well as from actual data. The data for the wind speed and air density from the FHWA database is called Modern-Era Retrospective analysis for Research and Applications (MERRA), which was released in 2018. The MATLAB code is attached in appendix C. From the numerical analysis, the velocity and air density are directly proportional to the power extraction but the velocity is more effective because during the calculation velocity is multiplied three times. We used distribution fitter tool in the MATLAB for the results of velocity, air density, and power extracted. The plots are shown in Figure 17 through Figure 19. The survival analysis is consistency studies in the engineering field. Figure 17 and Figure 18 show the consistency of the velocity and air density respectively.

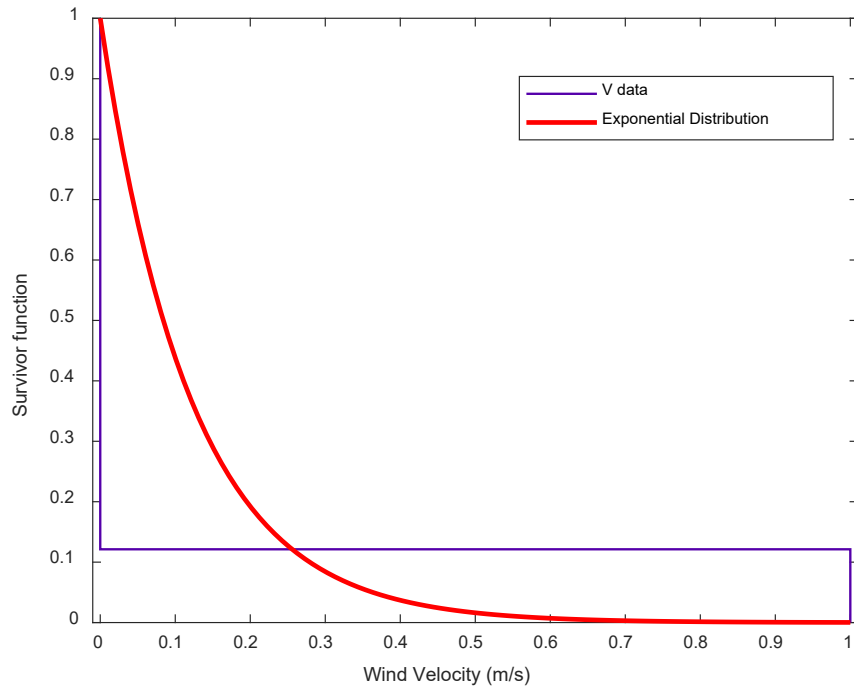


Figure 17 Distribution plot of wind velocity (V)

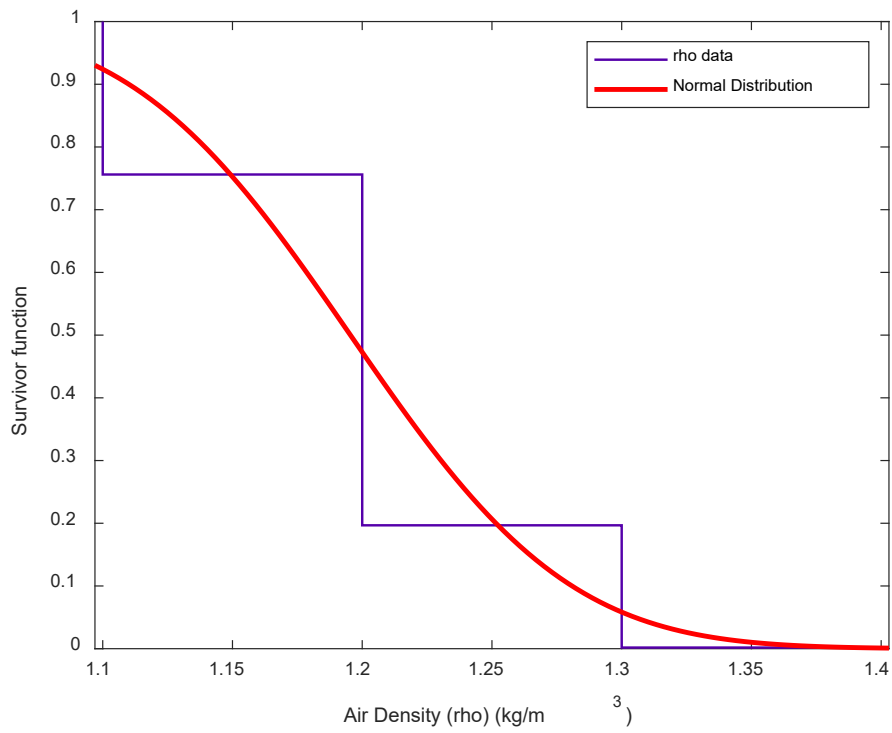


Figure 18 Distribution plot of air density rho

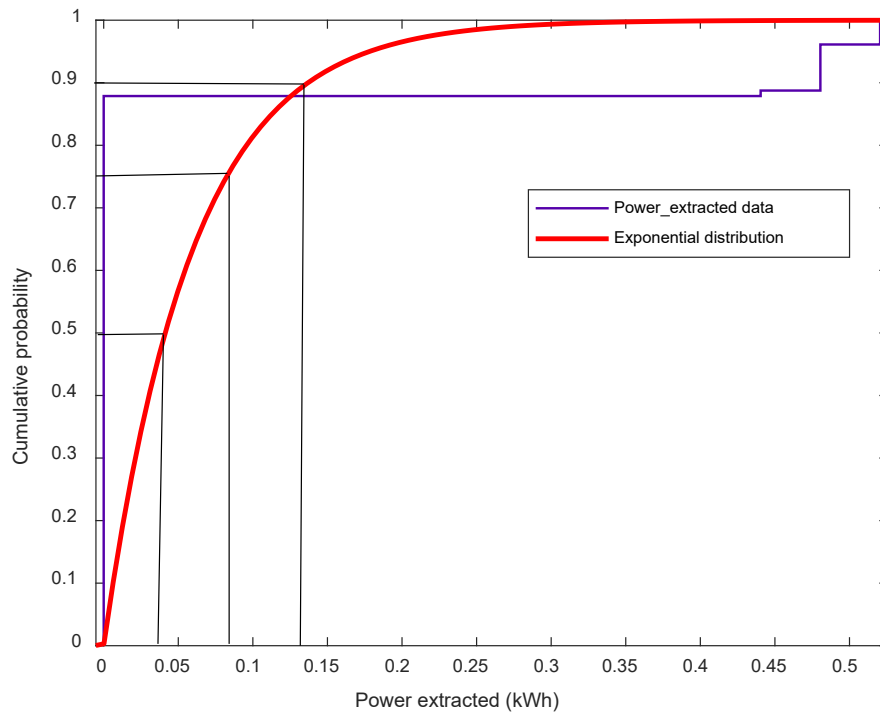


Figure 19 Distribution plot of power extracted from wind turbine

### Cost analysis

This section gives an explanation about the cost for different phases to develop this system on the road side that includes capital cost, operation cost, revenue, and overall cost per kWh. For the cost analysis, the calculation should be carried out for the levelized cost (net cost).

The Levelized Cost of the energy of the wind turbine is expressed as follows (Pan, et al., 2019):

$$COE = \frac{(FCR \times ICC)}{AEP_{net}} + AOE$$

26

Where, COE = levelized cost of energy (\$/kWh) (\$)

FCR = fixed charge rate (\$) (1/year)

ICC = initial capital cost (\$)

$AEP_{net}$  = net annual energy production (kWh/yr)

AOE = annual operating expense =  $LLC + (O\&M + LRC) / AEP_{net}$

LLC = Land Lease cost

O&M = levelized operation and management cost

LRC = levelized replacement/overhaul cost

The estimated initial capital cost is \$21,000 for ten wind turbines and the maintenance cost for each year is \$7000 (Bani-Hani, et al., 2018). According to past research, the normal annual operating expense of any wind turbine is \$5000. However, that cost has been calculated for very large wind turbine projects. For the wind turbine on the roadside, the approximate annual operating cost for ten helical wind turbines was assumed to be \$948 per year.

$$COE = \frac{(21000 * 7000)}{3500000} + 948 = \$980 /kWh \quad 27$$

The cash flow for the 10 wind turbines for 30 years is shown in Figure 20. In that graph, operation cost, net capital cost, and revenue is covered. The revenue is the tax that should be collected by the Federal government from the user based on current energy costs. The net cost influences with operation cost, revenue, and maintenance cost.

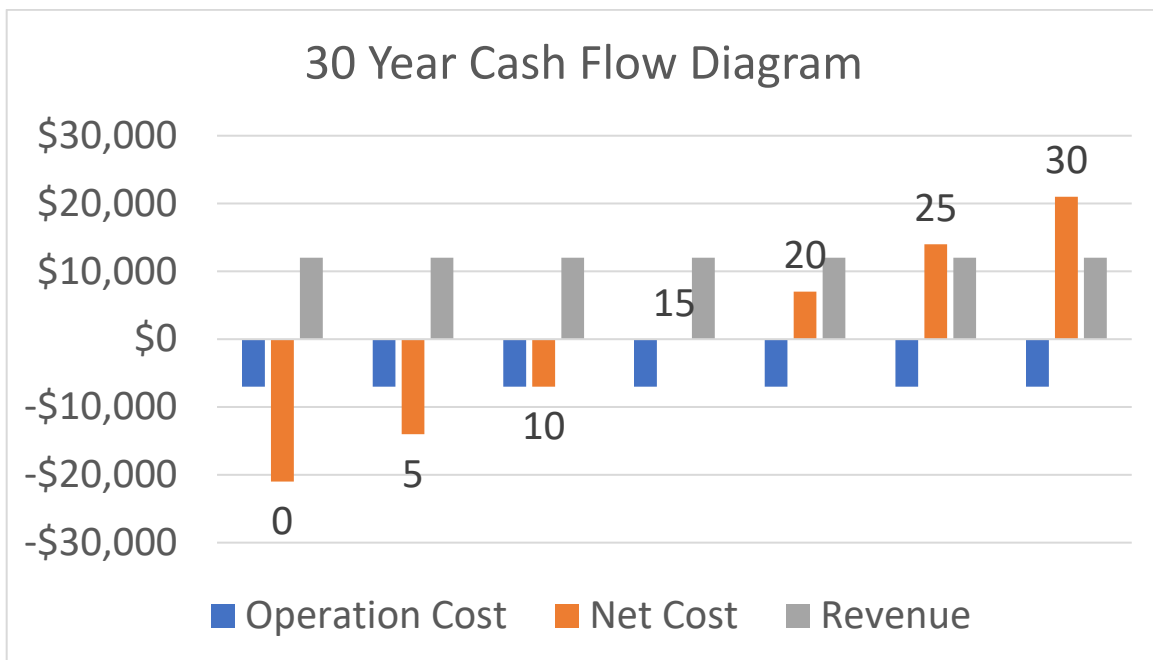


Figure 20 30-year Nominal Cash flow for wind turbine

## Solar roadway

A solar roadway is made up of three layers: base, electronic, and the tempered glass layer. In this type of road structure, asphalt is replaced by the tempered glass which is the main reason to not take it in consideration in this thesis because there is no previous research about how much friction can be achieved with that tempered glass. The brief detail about three layers is given in the following section.

### Conceptual Design of the solar roadway

A solar roadway could be a series of structurally engineered solar panels that are driven on. The concept is to replace current petroleum-based asphalt roads, parking lots and driveways with solar road panels that collect energy to be utilized by homes and businesses, and ultimately to be able to store excess energy in or alongside the solar roadways. Therefore, renewable energy replaces the need for the present fossil fuels used for the generation of electricity, which in turn reduces greenhouse gasses and helps in sustainable development. Parking lots, driveways and eventually highways are all targets for the panel (Mehta, Aggrawal, & Tiwari, 2015). If the whole United States interstate transportation system was surfaced with solar roadway panels, it would manufacture over 3 times the quantity of electricity presently used nationwide (Mehta et al., 2015). A Solar roadway consists of 3 layers as shown in Figure 21 and Figure 22.

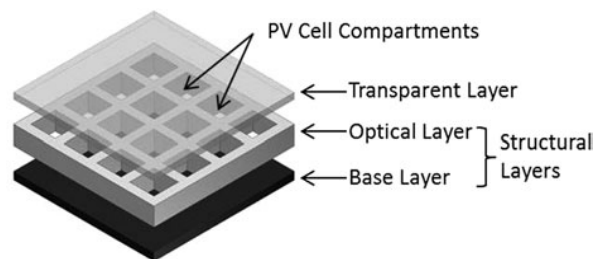


Figure 21 Three layers of solar roadway (Northmore & Tighe, 2016)

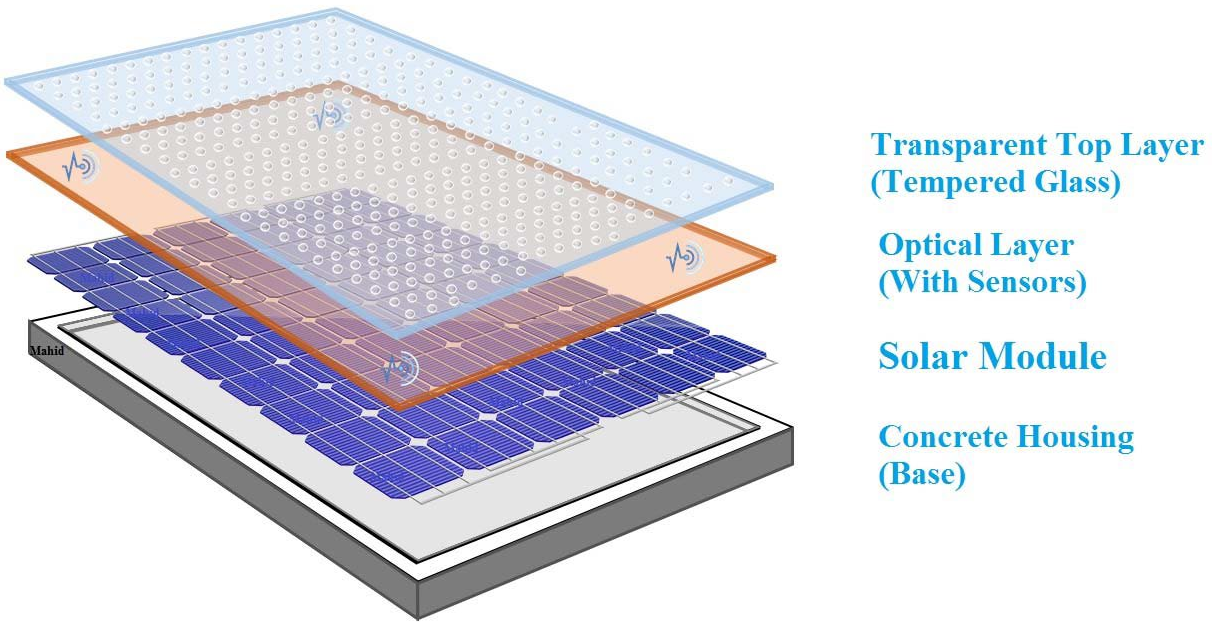


Figure 22 Layers of Solar Roadways (Rahman et al., 2017)

#### Road Surface layer

Translucent and high strength, it must have enough roughness to produce adequate friction, yet still passes daylight through to the reflector cells embedded among, at the side of LEDs and component. This layer must be capable of handling today's heaviest loads underneath the worst of conditions and to be weatherproof, to shield the electronic layer below it (Rahman et al., 2017). Usually, tampered glass is widely used as a transparent layer because of the smoothness and solidity of this glass. For the driving safety, there should be enough roughness in the surface to maintain the friction (Selvaraju, 2012).

#### Electronic layer

It contains photovoltaic cells that absorb solar energy. It additionally contains a small processor board with support circuit for sensing masses on the surface and a dominant heating element with a view to reducing or eliminating snow and ice removal, as well as college and business closings because of inclement weather. The microchip controls lighting communication that may be built into this pavement

and monitoring etc.

### Base Plate Layer

This layer must be able to protect the electronic layer from wet weather and helps to distribute power to and from the electronic panel.

### Analytical Analysis

The model for the solar panel is shown in Figure 23. The solar Irradiance (the flux of radiant energy per unit area) received by the solar cells is given as an input current to a voltage-controlled current source (Selvaraju, 2012). Current can be supported by the following equation:

$$I_L = \frac{i_{scm}}{1000} G \tag{28}$$

Where,  $I_L$  = photocurrent (the current which is produced by the sunlight)

$G$  = solar irradiance ( $W/m^2$ )

$i_{scm}$  = the measured short circuit current of solar module under standard condition

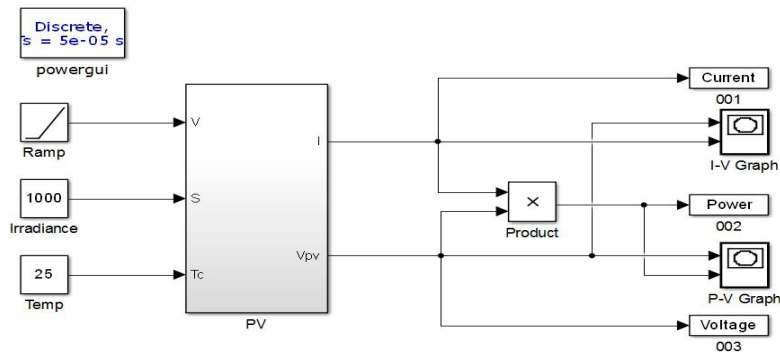


Figure 23 Model of solar panel (Rahman, Mahmud, Ahmed, Rahman, & Arif, 2017)

The series resistors placed into the model show the resistive losses in series which are existing in real solar panel. These losses mainly occur from the movement of currents which are generated by solar cells through the emitter, base of the cells, and partially due to the resistances. A series of resistive loss reduces the fill factor and the short circuit current of solar cells. The fill factor is the ratio of maximum obtainable power to the product of an open-circuit voltage and short circuit currents. Therefore, to include

shunt resistive losses, which are present in the actual solar panels, a shunt resistor should be included in the model. It might be noticed that shunt obstruction is likewise alluded to as parallel opposition. Shunt resistive losses are caused in the sun-powered cells principally because of assembling surrenders present in the sun-powered cells. Shunt resistive losses are additionally known to be bigger when the daylight falling over the sun-powered cells is at low levels (Selvaraju, 2012). To beat the current, a diode is incorporated into the proportional electrical circuit model. In this manner, the current (I) and voltage (V) attributes of the comparable electrical circuit of the sun-powered board depend on the equation 29:

$$I = I_L - I_0 \left( e^{\frac{v+IR_S}{nV_T}} - 1 \right) - \frac{v + IR_S}{R_{Sh}} \quad 29$$

Where I = output current

$I_0$  = Dark saturation current (Diode leakage current density in the absence of sunlight)

V = Voltage at output terminal

$R_S, R_{Sh}$  = Series and shunt resistance respectively

n = ideal diode factor (always between 1 and 2)

$V_T$  = thermal voltage according to the absolute temperature T in kelvin

Short circuit current for the comparable electrical circuit model of the sun-powered board is given by substituting  $V = 0$  (for example the yield voltage is being set to zero) in equation 30:

$$I_{SC} = I_L - I_0 \left( e^{\frac{v+IR_S}{nV_T}} - 1 \right) - \frac{v + IR_S}{R_{Sh}} \quad 30$$

Where  $I_{SC}$  = short circuit current of solar panel

Open circuit voltage for the proportionate electrical circuit of the solar panel is acquired by substituting  $I = 0$  (for example the yield voltage is set to zero) in equation 29. It is realized that the open-circuit voltage is autonomous of the series resistance value and furthermore the shunt obstruction value (Selvaraju, 2012). Consequently, those terms including the arrangement and shunt opposition value in the

equation 30 can be dismissed, for the open-circuit voltage  $V_{oc}$ :

$$V_{oc} = nV_T \ln \left( 1 + \frac{I_L}{I_0} \right) \quad 31$$

In a typical solar panel, several solar cells are connected in series and parallel. In order to model a solar panel into an equivalent electrical circuit, some assumptions must be made. The shunt resistance of the solar cells is assumed to be larger so that its effects can be neglected, and the photogenerated current  $I_L$  is assumed to be equal to that of the short circuit current  $I_{sc}$  of the solar cell (Selvaraju, 2012). The scaling rule for a solar panel where the number of cells in series is  $N_s$  and the number of cells in parallel is  $N_p$  results in:

$$I_M = N_p I , \quad I_{scM} = N_p I_{sc} \quad 32$$

$$V_M = N_s V , \quad V_{ocM} = N_s V_{oc} \quad 33$$

$$R_{sM} = \frac{N_s}{N_p} R_s \quad 34$$

In the above equations, the parameters with subscript M are used for the solar panel module, and without subscript, M is used for the single solar cell.

## Specification of Solar Panel

*Table 8 150W Poly Solar Panel Specification*

<b>Parameter</b>	<b>Value</b>
<b>Power (W)</b>	150
<b>Output tolerance</b>	± 3%
<b>Open Circuit Voltage (V)</b>	22.4
<b>Optimum Power (V)</b>	18
<b>Short circuit current (A)</b>	9.02
<b>Optimum current (A)</b>	8.33
<b>Dimension (m<sup>3</sup>)</b>	1.54*0.7150*0.006
<b>Temperature range (°C)</b>	-40 to 90
<b>Cost per unit (\$)</b>	220

*Table 9 300W Poly Solar Panel Specification (CS6K-300MS) Recommended*

<b>Parameter</b>	<b>Value</b>
<b>Power (W)</b>	300
<b>Output tolerance</b>	± 5%
<b>Open Circuit Voltage (V)</b>	39.70
<b>Optimum Power (V)</b>	32.50
<b>Short circuit current (A)</b>	9.83
<b>Optimum current (A)</b>	9.24
<b>Dimension (m<sup>3</sup>)</b>	1.65*0.992*0.04
<b>Temperature range (°C)</b>	-40 to 85
<b>Cost per unit (\$)</b>	178

According to our location, the maximum 8352 solar panels are needed including only the walkways. However, after the analysis of all the possible energy harvesting sources, the solar panel is less compatible and economical as compared to the other two sources piezoelectric and wind turbine.

## CHAPTER 5 DISCUSSION AND CONCLUSION

### Discussion

According to the potential calculation of different energy harvest sources, piezoelectric is the most efficient source to generate energy from the pavement. The potential energy production calculations cover the cost and benefit ratio. In this thesis, I have covered the equation to calculate the estimation of energy production and the cost to produce that energy through the specific energy harvesting source. However, the estimation of the amount of energy harvesting from any source depends on capital investment, installation charge, operation, and management cost, and cost per kWh. This thesis is not advocating solar energy harvesting method at this time because solar roadways have been proposed but the solar roadways with glass surface as a top layer in the roads can resist the vehicle 80 mile/hr without skidding and that has not been proved. However, no paper has been published about it, so I have not covered it in my paper.

Piezoelectric was shown to be a good source to harvest the energy from the asphalt pavement. Specifically, it is feasible in urban areas because piezoelectric is inversely proportional to the vehicle speed. So, due to the high traffic density in urban area the energy production potential is significant. There are three types of piezoelectric transducers available; Cymbal, Bridge, and Moonie. In this thesis we considered cymbal because of the loading condition and efficiency under the asphalt pavement. From Table 4 and Table 5, the increment in energy production was found to be approximately 250 kWh because of the strains. After a cross-check with the energy usage of the Weisberg Arthur Engineering Building which is located on 3<sup>rd</sup> Avenue in Huntington, I found that we can produce the energy that can be used for an engineering building. The cost to produce the energy from the piezoelectric material is \$1.44/kWh. This cost includes the maintenance cost and installation cost throughout the life span of the piezoelectric transducers.

An important note is that I have compared the use of the Winkler's foundation equation to an empirical formula for the asphalt pavement strains. The main reason for comparison of two approaches is strain does not behave like a Winkler foundation in asphalt pavement, but it is unknown how the addition of piezoelectric sensors will affect this. For all the calculation for the piezoelectric output we used MATLAB for more accuracy with the results, and the MATLAB code is attached in appendix B, C, and D.

### **Advantages of Piezoelectric materials**

In addition to power generation, piezoelectric sensors provide other potential benefits including:

1. Piezoelectric transducers have sensors which can help to measure the pavement condition as well as the base layer condition if it is in contact with both surfaces.
2. If the piezoelectric circuit has coil base coupling, then it can help to melt down the snow during the winter season.
3. It is the most economical way to harvest energy from the pavements.

### **Disadvantages of Piezoelectric materials**

1. The set up under the existing roads is difficult.
2. If the coil base coupling is using for the collection of power, then we must provide sufficient heat to absorb material around the coil to protect the asphalt layer.
3. The sensors can be damaged when the asphalt layer is damaged and replacement of damaged sensors would require damage to the pavement.

The wind turbine is another alternative to produce energy from the roadside. However, there are different types of wind turbines available in the market, but for the specific location, after analysis helical VAWT turbine is more efficient than a normal vertical wind turbine. In this situation, the wind turbine is placed into the lighting pole on the roadside, due to efficiency concern the radius of the rotor should be sufficient larger than the height of the rotor. In this case, we have calculated the wind speed of air. The

energy cost products from the wind turbine are \$980 /kWh including all the maintenance, operation and management costs.

There are many benefits and drawbacks to employing a vertical turbine design. The vertical turbine design is chosen as a result of vertical turbines being able to capture the wind in any direction, whereas, horizontal turbines ought to be pointed within the direction of the wind.

### **Advantages of VAWT**

1. It is cheaper to produce the electricity than the horizontal axis wind turbine.
2. It can be installed more easily than the horizontal axis wind turbine.
3. Lessening the risk to people and local birds because it is equipped with the low-speed blades.
4. It can work in extreme weather.

### **Disadvantages of VAWT**

1. It has higher vibrations due to turbulent flow of air near the ground.
2. Bearing wear increases due to vibrations that increase the maintenance cost.
3. It may create noise pollution.

### **Conclusion**

For the analysis, MATLAB tool is helpful for the accurate Monte Carlos simulation. For both sources, the calculation has been done with distribution by MATLAB coding. In this paper, the estimation of both source piezoelectric material and wind turbine has been calculated with the help of Levelized cost. Levelized cost covered all capital, maintenance, and leasing costs which provides more complete cost information. After output analysis and the cost simulation for the two harvesting sources, theoretically, it is feasible and potentially beneficial for the specific location investigated.

The piezoelectric material is good harvesting sourced from the asphalt pavement as compared to others because the potential benefits of the piezoelectric are more than a wind turbine. However, it is a

time consuming and expensive process to implement on existing roads because of labor work. Also, Piezoelectric material produces the heat and asphalt is a temperature sensitive material. So, for that, you must have arrangements to maintain the temperature or reuse that heat to generate energy. For future recommendation, the heat can be used to produce more electricity through the photovoltaic plate.

The initial cost for the wind turbine is much higher than the piezoelectric material but it is more feasible along the highways as compared to specific locations. The 3rd Avenue of Huntington has parking on both sides of the road, so the wind which is generated by the moving vehicle cannot be considered in that case. Also, in this case, land leasing cost should not be considered for estimation but this paper covered it for the general idea of the cost of a wind turbine on the roadside light pole.

## REFERENCES

- Andriopoulou, S. (2012). A review on energy harvesting from roads. *MSc Environmental Engineering \& Sustainable Infrastructure, [TSC-MT 12-017], KTH Royal Institute of Technology*.
- Bani-Hani, E. H., Sedaghat, A., AL-Shemmary, M., Hussain, A., Alshaieb, A., & Kakoli, H. (2018). Feasibility of Highway Energy Harvesting Using a Vertical Axis Wind Turbine. *Energy Engineering, 115*(2), 61-74.
- Bansal, P. (2015). Charging of Electric Vehicles: Technology and Policy Implications. *Journal of Science Policy & Governance, 6*, 1-20.
- Bryce, J., Elkins, G., & Thompson, T. (2019). Sensitivity analysis of Highway Economic Requirements System Pavement Performance Models. *Journal of Transportation Engineering Part B: Pavements*.
- Caliò, R., Rongala, U., Camboni, D., Milazzo, M., Stefanini, C., De Petris, G., & Oddo, C. (2014). Piezoelectric Energy Harvesting Solutions. *Sensors*.
- Champagnie, B., Altenor, G., & Simonis, A. (2013). *Highway Wind Turbines*. Florida.
- Duarte, F., Casimiro, F., Correia, D., Mendes, R., & Ferreira, A. (2003). A new pavement energy harvest system. 408-413.
- FHWA. (2019, August). *LTPP Infopave: Visualization*. Retrieved from Infopave: <https://infopave.fhwa.dot.gov/Media/LTPPSectionMapping>
- Guo, L., & Lu, Q. (2017). Potentials of piezoelectric and thermoelectric technologies for harvesting energy from pavements. *Renewable and Sustainable Energy Reviews, 72*, 761-773.
- Harald, B., Sreedhar, K., Ulrich, G., Reinaldo, R.-R., Raul, G., Jose, O. A., & Julian, B.-C. (2005). An analytical and numerical approach for calculating effective material coefficients of piezoelectric fiber composites. *International Journal of Solids and Structures, 42*(21-22), 5692-5714. doi:<https://doi.org/10.1016/j.ijsolstr.2005.03.016>
- Hu, W., Jiaqiang, E., Deng, Y., Li, L., Han, D., Zhao, X., . . . Peng, Q. (2018). Effect analysis on power coefficient enhancement of a convective wind energy collecting device in the expressway. *Energy conversion and management, 171*, 248-271.
- Ilyas, M. A. (2018). *Piezoelectric Energy Harvesting: Methods, Progress, and Challenges*. New York: Momentum Press, LLC, New York.
- Jasim, A., Wang, H., Yesner, G., Safari, A., & Maher, A. (2017). Optimized design of layered bridge transducer for piezoelectric energy harvesting from roadway. *Energy, 141*, 1133-1145.
- Jasim, A., Yesner, G., Wang, H., Safari, A., Maher, A., & Basily, B. (2018). Laboratory testing and numerical simulation of piezoelectric energy harvester for roadway applications. *Applied energy, 224*, 438-447.
- Kang, I., Heung, Y., Kim, J. H., Lee, J., Gollapudi, R., Subramaniam, S., . . . Ruggles-Wren, M. (2006). Introduction to carbon nanotube and nanofiber smart materials. *Composites Part B: Engineering, 37*(6), 382-394. doi:<https://doi.org/10.1016/j.compositesb.2006.02.011>.

- Kothe, L. B., Moller, S. V., & Petry, A. P. (2019). Numerical and experimental study of a helical Savonius wind turbine and a comparison with a two-stage Savonius turbine. *Renewable Energy*, 1-49.
- Ltd., A. I. (2011). *Piezoelectric Ceramics: Principles and Applications*. APC International Ltd.
- Malave, S. N., & Bhosale, S. P. (2013). Highway Wind Turbine (Quite Revolution Turbine). *International Journal of Engineering Research and Technology*, 6, 789-794.
- Mazharul, I., David, T. S.-K., & Amir, F. (2006). Aerodynamic models for Darrieus-type straight-bladed vertical axis wind turbines. *Renewable and Sustainable Energy Reviews*, 12(4), 1087-1109.  
doi:<https://doi.org/10.1016/j.rser.2006.10.023>
- Mehta, A., Aggrawal, N., & Tiwari, A. (2015). Solar Roadways-The future of roadways. *International Advanced Research Journal in Science, Engineering and Technology (IARJSET)*.
- Moure, A., Rodriguez, M. I., Rueda, S. H., Gonzalo, A., Rubio-Marcos, F., Cuadros, D. U., . . . Fernandez, J. (2016). Feasible integration in asphalt of piezoelectric cymbals for vibration energy harvesting. *Energy conversion and management*, 112, 246-253.
- Najini, H., & Muthukumaraswamy, S. A. (2016). Investigation on the selection of piezoelectric materials for the design of an energy harvester system to generate energy from traffic. *International Journal of Engineering and Applied Sciences*.
- Najini, H., & Muthukumaraswamy, S. A. (2017). Piezoelectric energy generation from vehicle traffic with techno-economic analysis. *Journal of Renewable Energy*.
- Nakil, K., Tekale, A., Sambhus, P., & Patil, R. (2016). Analysis of Vertical Axis Windmill Turbine for Electricity Generation on Highways. *International Journal of Current Engineering and Technology*, 6, 113-119.
- Northmore, A. B., & Tighe, S. L. (2016). Performance modelling of a solar road panel prototype using finite element analysis. *International Journal of Pavement Engineering*, 17(5), 449-457.
- Pan, H., Li, H., Zhang, T., Laghari, A. A., Zhang, Z., Yuan, Y., & Qian, B. (2019). A portable renewable wind energy harvesting system integrated S-rotor and H-rotor for self-powered applications in high-speed railway tunnels. *Energy Conversion and Management*, 196, 56-68.
- Rahman, M. W., Mahmud, M. S., Ahmed, R., Rahman, M. S., & Arif, M. Z. (2017). Solar lanes and floating solar PV: New possibilities for source of energy generation in Bangladesh. In *2017 Innovations in Power and Advanced Computing Technologies (i-PACT)* (pp. 1-6).
- Reddy, J. N. (2006). *Theory and analysis of elastic plates and shells*. CRC press.
- Selvaraju, R. K. (2012). Characterization of Solar Roadways Via Computational and Experimental Investigations. *Electronic Thesis and Dissertation Repository*.
- Tong, W. (2010). *Wind power generation and wind turbine design*. WIT press.
- Xu, X., Cao, D., Yang, H., & He, M. (2018). Application of piezoelectric transducer in energy harvesting in pavement. *International Journal of Pavement Research and Technology*, 11, 288-295.

- Yesner, G., Jasim, A., Wang, H., Basily, B., Maher, A., & Safari, A. (2019). Energy harvesting and evaluation of a novel piezoelectric bridge transducer. *Sensors and Actuators A: physical*, 285, 348-354.
- Zhang, Z., Xiang, H., & Shi, Z. (2016). Modeling on piezoelectric energy harvesting from pavements under traffic loads. *Journal of Intelligent Material Systems and Structures*, 27, 567-578.
- Zhao, H., Ling, J., & Yu, J. (2012). A comparative analysis of piezoelectric transducers for harvesting energy from asphalt pavement. *Journal of the Ceramic Society of Japan*, 120, 317-323.
- Zhao, H., Tao, Y., Niu, Y., & Ling, J. (2014). Harvesting energy from asphalt pavement by piezoelectric generator. *Journal of Wuhan University of Technology-Mater. Sci. Ed.*, 29(5), 933-937.

## APPENDIX A APPROVAL LETTER



Office of Research Integrity

November 13, 2019

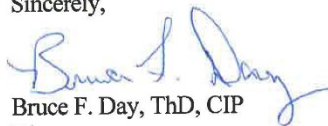
Dhruvalkumar Hitendrakumar Patel  
2100 7<sup>th</sup> Avenue, Apt #413  
Huntington, WV 25703

Dear Dhruvalkumar:

This letter is in response to the submitted thesis abstract entitled "*Smart Roads: Investigating Roadways as Energy Sources for Potential Application of In-Lane Charging.*" After assessing the abstract, it has been deemed not to be human subject research and therefore exempt from oversight of the Marshall University Institutional Review Board (IRB). The Code of Federal Regulations (45CFR46) has set forth the criteria utilized in making this determination. Since the information in this study does not involve human subjects as defined in the above referenced instruction, it is not considered human subject research. If there are any changes to the abstract you provided then you would need to resubmit that information to the Office of Research Integrity for review and a determination.

I appreciate your willingness to submit the abstract for determination. Please feel free to contact the Office of Research Integrity if you have any questions regarding future protocols that may require IRB review.

Sincerely,



Bruce F. Day, ThD, CIP  
Director

**WE ARE... MARSHALL.**

One John Marshall Drive • Huntington, West Virginia 25755 • Tel 304/696-4303  
A State University of West Virginia • An Affirmative Action/Equal Opportunity Employer

## APPENDIX B MATLAB CODING FOR PIEZOELECTRIC TRANSDUCERS

```

clc
syms m x t y
rho=2323;
h=0.3048;
E=27560*10^6;
mu=0.15;
B=8;
K=136;
N=20;
Massofvehicle=3200;
coeffofrollingfriction=0.015;
Contacttires=2;
areaofcontact=0.0025;
v=(30*5)/18; %assumng 30mile/hr
b0=.508/2;
a0=0.254/2;
d0=1.22/2;
q0= Massofvehicle*coeffofrollingfriction*Contacttires/(areaofcontact*v)%-7.78?10?3;
%distributed load of vehicle
y1=3.2;
y2=4.8;
%piezo
d31=-274*10^(-12); %V/m
hc=0.055;
lp=0.14;
bp=0.14;
hp=0.02;
e33=30.06*10^(-9); % F/m
S11=16.5*10^(-12); %m?2/N
S12=-5.74*10^(-12); %m?2/N
xp=8;%tenative
yp=0.5;%centre of piezo
R =800*10^3;
xp1=xp-0.5*lp;
xp2=xp+0.5*lp;
yp1=yp-0.5*bp;
yp2=yp+0.5*bp;
%pavement structuring
D=E*h/(12*(1-mu^2));
am=m*sym(pi)/B;
a1=sym(pi)/9.8814; %supposed to be B
vc=sqrt((2*(a1^2)*D+2*sqrt((a1^4)*D^2+K*D))/(rho*h));
Lm=sqrt(am^4+K/D);
Bm=((v^2)*rho*h/(2*D))-am^2;

```

```

Tm=sqrt(0.5*(Lm-Bm));
Pm=sqrt(0.5*(Lm+Bm));
v0=sqrt((4*D*am^2)/(rho*h));
o=(2*v^2-v0^2)/(2*sqrt((vc^2-v^2)*(v^2+vc^2-v0^2))); %gamma m
deg=180/pi;
cm1=((o*sin(a0*Pm)*cosh(a0*Tm)+cos(a0*Pm)*sinh(a0*Tm)));
sm1=(-o*cos(a0*Pm)*sinh(a0*Tm)+sin(a0*Pm)*cosh(a0*Tm));
cm2=((exp(-a0*Tm))*(o*sin(a0*Pm)-cos(a0*Pm)));
sm2=(-exp(-a0*Tm))*(o*cos(a0*Pm)+sin(a0*Pm));
CM2=((exp(-d0*Tm))*(cm1*cos(d0*Pm)+sm1*sin(d0*Pm)));
SM2=((exp(-d0*Tm))*(sm1*cos(d0*Pm)-cm1*sin(d0*Pm)));
CM1=((exp(d0*Tm))*(cm1*cos(d0*Pm)-sm1*sin(d0*Pm))+CM2);
SM1=((exp(d0*Tm))*(cm1*sin(d0*Pm)+sm1*sin(d0*Pm))+SM2);
CM3=(cm2*cos(d0*Pm)*cosh(d0*Tm)+sm2*sin(d0*Pm)*sinh(d0*Tm));
CM4=(-cm2*cos(d0*Pm)*sinh(d0*Tm)-sm2*sin(d0*Pm)*cosh(d0*Tm));
SM3=(cm2*sin(d0*Pm)*cosh(d0*Tm)-sm2*cos(d0*Pm)*sinh(d0*Tm));
SM4=(sm2*cos(d0*Pm)*cosh(d0*Tm)-cm2*sin(d0*Pm)*sinh(d0*Tm));
O=abs(x-v*t);
gm1=((cosh(O*Tm))*(CM3*cos(O*Pm)+SM3*sin(O*Pm)));
gm2=((sinh(O*Tm))*(CM4*cos(O*Pm)+SM4*sin(O*Pm)));
gm=(gm1+gm2);
wm=((4*q0*sin(am*b0)*(sin(am*y1)+sin(am*y2)))/(m*pi*(K+D*am^4)));
%case 1 when O-d0>a0
wm1=(wm*(exp(-O*Tm))*(CM1*cos(O*Pm)+SM1*sin(O*Pm)));
%case 2 when |O-d0| <a0
wm2=(wm*(1+(exp(-O*Tm))*(CM2*cos(O*Pm)+SM2*sin(O*Pm))+gm));
%case 3 when (O-d0<-a0)
wm3=(wm*(2*CM2*cos(O*Pm)*cosh(O*Tm)-2*SM2*sin(O*Pm)*sinh(O*Tm)));
C0=(e33-(1/(S11+S12))*2*d31^2)*lp*bp/hp;
syms m
WM1=(symsum(wm1*sin(am*y), m, 1, N));
WM2=(symsum(wm2*sin(am*y), m, 1, N));
WM3=(symsum(wm3*sin(am*y), m, 1, N));
WM=WM1+WM2+WM3;
WM=vpa(WM,3);
gx=gradient(WM,x);
gx=vpa(gx,3)
gy=gradient(WM,y);
gy=vpa(gy,3)
gy1=gradient(gy);
gy1=vpa(gy1,3);%deba2w(x,y,t)wrt y
fun=vpa((gx+gy),3);
term=vpa(int(fun,x),3); %first integral
initial=subs(term,x,xp1); %limits
final=subs(term,x,xp2);
term=vpa((final-initial),3);

```

```

TERM=vpa(int(term,y),3);
initial1=subs(TERM,y,yp1); %limits
final1=subs(TERM,y,yp2);
TERM=vpa((final1-initial1),3);
Q=-((d31*hc)/(S11+S12))*TERM; %fill up the two integrals
ex=-hc*gx1;
ex=vpa(ex,3);
ey=-hc*gy1;
ey=vpa(ey,3);
e31=d31/(S11+S12);
V= e31*lp*bp*(ex+ey)/C0;
% for y=8 t=8/30
V=subs(V,y,8);
V=subs(V,t,8/30);
V=subs(V,x,1);
V=vpa(V,2)
AA=int((Q*exp(t/R*C0)),t);
Vt=(Q/C0)-((1/R*C0^2)*(exp(-t/(R*C0)))*(AA));
Vt1=vpa(Vt,2)
Vt1=subs(Vt1,t,8/30)

```

## APPENDIX C MATLAB CODING FOR SENSITIVITY ANALYSIS

```
%For the sensitivity analysis
run gdat.m
size=3; %size of the variables
% rt=0.03; %growth rate for traffic (backwards prediction)
% baseind=0; % use 1 for granular, and 0 for stiffer base (e.g., CTB)
%
% [Age, ESALS, lane_width, speed_limit, Subgrade_ResilientMod, Sand_Fraction, Silt_Fraction,
Clay_Fraction, Plast_Ind, MAAT, rain, Freeze_Ind, Freeze_Thaw, Depth_GWT, HMA_Voids,
HMA_BindCont, Perc_34, Perc_38, Perc_No4, Perc_No80, Perc_No200, Bind_VTS, Bind_A, Base_Mod,
ACThck, BaseThck]=ACDatafunc(size, rt, baseind);

%[size, Age, ESALS, lane_width, speed_limit, Subgrade_ResilientMod, Sand_Fraction, Silt_Fraction,
Clay_Fraction, Plast_Ind, MAAT, rain, Freeze_Ind, Freeze_Thaw, Depth_GWT, HMA_Voids,
HMA_BindCont, Perc_34, Perc_38, Perc_No4, Perc_No80, Perc_No200, Bind_VTS, Bind_A, Base_Mod,
ACThck, BaseThck]=AC_Check(size, Age, ESALS, lane_width, speed_limit, Subgrade_ResilientMod,
Sand_Fraction, Silt_Fraction, Clay_Fraction, Plast_Ind, MAAT, rain, Freeze_Ind, Freeze_Thaw,
Depth_GWT, HMA_Voids, HMA_BindCont, Perc_34, Perc_38, Perc_No4, Perc_No80, Perc_No200,
Bind_VTS, Bind_A, Base_Mod, ACThck, BaseThck);

mat=zeros(size,14);
for i=1:size

    [Estar, nu]=HMA_DynMod(speed_limit(i), Perc_No200(i), Perc_No4(i), Perc_38(i), Perc_34(i),
HMA_Voids(i), HMA_BindCont(i), Bind_A(i), Bind_VTS(i), MAAT(i));
    mat(i,1)=Estar;
    mat(i,2)=nu;

    [Strain_Horiz_BottHMA, Strain_Vert_MidHMA, Strain_Vert_TopSUBGR, Strain_Vert_MidBASE,
ACThk, BaseThk]=HMA_CriticalStains(Estar, BaseThck(i), ACThck(i), Base_Mod(i),
Subgrade_ResilientMod(i));
    mat(i,3)=Strain_Horiz_BottHMA;
    mat(i,4)=Strain_Vert_MidHMA;
    mat(i,5)=Strain_Vert_TopSUBGR;
    mat(i,6)=Strain_Vert_MidBASE;

end

mat(:,4)
```

## APPENDIX D MATLAB CODING FOR VAWT ANALYSIS

```
clc
R=0.70; %rotor radius
H=1.43; %height of rotor
A=2*R*H; %area of the wind turbine
Cp=0.4; %overall efficiency of wind turbine
% rho=1.225; %air density
size=17;
V = xlsread('velocity.xlsx','Sheet1','a2:a6721');
rho=xlsread('velocity.xlsx','Sheet1','b2:b6721');
Power_extracted=(rho.*Cp.*A.*V.^3)./2;
size=1e6;
a=randn(size,3);
ad1=makedist('Normal',0,1); a1 = cdf(ad1,a(:,1));
pd2 = makedist('Beta',2,5);New_Cp = icdf(pd2,a1);
hist(0.4.*New_Cp+0.2,25)

ad1=makedist('Normal',0,1); a1 = cdf(ad1,a(:,2));
pd2 = makedist('Exponential',0.09); V2 = icdf(pd2,a1);
hist(5.*V2+1,25)

ad1=makedist('Normal',0,1); a1 = cdf(ad1,a(:,3));
pd2 = makedist('Exponential',0.09); rho2 = icdf(pd2,a1);
hist(0.3.*rho2+1.1,25)

a2=round(rand(size,3).*(length(V)-1)+1);

for i=1:size;
    Cp2=New_Cp(a2(i,1));
    V21=V2(a2(i,1));
    rho22=rho2(a2(i,1));
    Power_extracted2(i)=(rho22.*Cp2.*A.*V21.^3)./2;
end
```

## APPENDIX E PERMISSION CERTIFICATES

10/1/2019

RightsLink Printable License

### ELSEVIER LICENSE TERMS AND CONDITIONS

Oct 01, 2019

---

This Agreement between 314 Myers avenue ("You") and Elsevier ("Elsevier") consists of your license details and the terms and conditions provided by Elsevier and Copyright Clearance Center.

License Number	4680540094919
License date	Oct 01, 2019
Licensed Content Publisher	Elsevier
Licensed Content Publication	Applied Energy
Licensed Content Title	Laboratory testing and numerical simulation of piezoelectric energy harvester for roadway applications
Licensed Content Author	Abbas Jasim,Greg Yesner,Hao Wang,Ahmad Safari,Ali Maher,B. Basily
Licensed Content Date	Aug 15, 2018
Licensed Content Volume	224
Licensed Content Issue	n/a
Licensed Content Pages	10
Start Page	438
End Page	447
Type of Use	reuse in a thesis/dissertation
Portion	figures/tables/illustrations
Number of figures/tables/illustrations	1
Format	both print and electronic
Are you the author of this Elsevier article?	No
Will you be translating?	Yes, including English rights
Number of languages	1
Languages	English
Original figure numbers	figure 5
Title of your thesis/dissertation	Smart roads: In-lane charging
Expected completion date	Dec 2019
Estimated size (number of pages)	55
Requestor Location	314 Myers avenue 314 Myers avenue  BECKLEY, WV 25801 United States Attn: 314 Myers avenue
Publisher Tax ID	98-0397604

<https://s100.copyright.com/AppDispatchServlet>

1/6



- Home
- Account Info
- Help



**Title:** Modeling on piezoelectric energy harvesting from pavements under traffic loads

**Author:** Zhiwei Zhang, Hongjun Xiang, Zhifei Shi

**Publication:** Journal of Intelligent Material Systems and Structures

**Publisher:** SAGE Publications

**Date:** 03/01/2016

Copyright © 2016, © SAGE Publications

Logged in as:  
Dhruvankumar Patel  
Account #: 3001528235

LOGOUT

**Gratis Reuse**

Permission is granted at no cost for use of content in a Master's Thesis and/or Doctoral Dissertation. If you intend to distribute or sell your Master's Thesis/Doctoral Dissertation to the general public through print or website publication, please return to the previous page and select 'Republish in a Book/Journal' or 'Post on intranet/password-protected website' to complete your request.

BACK

CLOSE WINDOW

Copyright © 2019 Copyright Clearance Center, Inc. All Rights Reserved. [Privacy statement](#). [Terms and Conditions](#). Comments? We would like to hear from you. E-mail us at [customercare@copyright.com](mailto:customercare@copyright.com)



# RightsLink®

[Home](#)[Create Account](#)[Help](#)

**Taylor & Francis**  
Taylor & Francis Group

**Title:** Performance modelling of a solar road panel prototype using finite element analysis

**Author:** Andrew B. Northmore, , Susan L. Tighe

**Publication:** International Journal of Pavement Engineering

**Publisher:** Taylor & Francis

**Date:** May 27, 2016

Rights managed by Taylor & Francis

**LOGIN**

If you're a [copyright.com user](#), you can login to RightsLink using your copyright.com credentials. Already a [RightsLink user](#) or want to [learn more?](#)

### Thesis/Dissertation Reuse Request

Taylor & Francis is pleased to offer reuses of its content for a thesis or dissertation free of charge contingent on resubmission of permission request if work is published.

[BACK](#)[CLOSE WINDOW](#)

Copyright © 2019 [Copyright Clearance Center, Inc.](#) All Rights Reserved. [Privacy statement](#). [Terms and Conditions](#).  
Comments? We would like to hear from you. E-mail us at [customerscare@copyright.com](mailto:customerscare@copyright.com)



# RightsLink®

[Home](#)
[Create Account](#)
[Help](#)


**Title:** Solar lanes and floating solar PV: New possibilities for source of energy generation in Bangladesh

**Conference Proceedings:** 2017 Innovations in Power and Advanced Computing Technologies (I-PACT)

**Author:** Md Wazedur Rahman

**Publisher:** IEEE

**Date:** April 2017

Copyright © 2017, IEEE

#### LOGIN

If you're a [copyright.com](#) user, you can login to RightsLink using your copyright.com credentials. Already a [RightsLink](#) user or want to [learn more?](#)

### Thesis / Dissertation Reuse

**The IEEE does not require individuals working on a thesis to obtain a formal reuse license, however, you may print out this statement to be used as a permission grant:**

*Requirements to be followed when using any portion (e.g., figure, graph, table, or textual material) of an IEEE copyrighted paper in a thesis:*

- 1) In the case of textual material (e.g., using short quotes or referring to the work within these papers) users must give full credit to the original source (author, paper, publication) followed by the IEEE copyright line © 2011 IEEE.
- 2) In the case of illustrations or tabular material, we require that the copyright line © [Year of original publication] IEEE appear prominently with each reprinted figure and/or table.
- 3) If a substantial portion of the original paper is to be used, and if you are not the senior author, also obtain the senior author's approval.

*Requirements to be followed when using an entire IEEE copyrighted paper in a thesis:*

- 1) The following IEEE copyright/ credit notice should be placed prominently in the references: © [year of original publication] IEEE. Reprinted, with permission, from [author names, paper title, IEEE publication title, and month/year of publication]
- 2) Only the accepted version of an IEEE copyrighted paper can be used when posting the paper or your thesis on-line.
- 3) In placing the thesis on the author's university website, please display the following message in a prominent place on the website: In reference to IEEE copyrighted material which is used with permission in this thesis, the IEEE does not endorse any of [university/educational entity's name goes here]'s products or services. Internal or personal use of this material is permitted. If interested in reprinting/republishing IEEE copyrighted material for advertising or promotional purposes or for creating new collective works for resale or redistribution, please go to [http://www.ieee.org/publications\\_standards/publications/rights/rights\\_link.html](http://www.ieee.org/publications_standards/publications/rights/rights_link.html) to learn how to obtain a License from RightsLink.

If applicable, University Microfilms and/or ProQuest Library, or the Archives of Canada may supply single copies of the dissertation.

[BACK](#)
[CLOSE WINDOW](#)

Copyright © 2019 Copyright Clearance Center, Inc. All Rights Reserved. [Privacy statement](#). [Terms and Conditions](#). Comments? We would like to hear from you. E-mail us at [customercare@copyright.com](mailto:customercare@copyright.com)

**ELSEVIER LICENSE  
TERMS AND CONDITIONS**

Nov 09, 2019

---

This Agreement between Mr. Dhruvalkumar Patel ("You") and Elsevier ("Elsevier") consists of your license details and the terms and conditions provided by Elsevier and Copyright Clearance Center.

License Number	4705060079114
License date	Nov 09, 2019
Licensed Content Publisher	Elsevier
Licensed Content Publication	Renewable Energy
Licensed Content Title	Numerical and experimental study of a helical Savonius wind turbine and a comparison with a two-stage Savonius turbine
Licensed Content Author	Leonardo Brito Kothe,Sérgio Viçosa Möller,Adriane Prisco Petry
Licensed Content Date	Available online 31 October 2019
Licensed Content Volume	n/a
Licensed Content Issue	n/a
Licensed Content Pages	1
Start Page	0
End Page	0